Coupled Systems Mechanics, *Vol. 4, No. 1 (2015) 67-98*
DOI: http://dx.doi.org/10.12989/csm.2015.4.1.067

Solution verification procedures for modeling and simulation of fully coupled porous media: static and dynamic behavior

Panagiota Tasiopoulou[1a], Mahdi Taiebat[2b], Nima Tafazzoli[3c] and Boris Jeremić[*4]

[1]*National Technical University of Athens, Athens, Greece*
[2]*Department of Civil Engineering, The University of British Columbia, Vancouver, BC, Canada*
[3]*Tetra Tech EBA, Vancouver, BC, Canada*
[4]*Department of Civil and Environmental Engineering, University of California, Davis, CA, USA and Earth Science Division, Lawrence Berkeley National Laboratory, Berkeley, CA, USA*

(Received September 25, 2014, Revised January 20, 2015, Accepted February 3, 2015)

Abstract. Numerical prediction of dynamic behavior of fully coupled saturated porous media is of great importance in many engineering problems. Specifically, static and dynamic response of soils – porous media with pores filled with fluid, such as air, water, etc. – can only be modeled properly using fully coupled approaches. Modeling and simulation of static and dynamic behavior of soils require significant Verification and Validation (V&V) procedures in order to build credibility and increase confidence in numerical results. By definition, Verification is essentially a mathematics issue and it provides evidence that the model is solved correctly, while Validation, being a physics issue, provides evidence that the right model is solved. This paper focuses on Verification procedure for fully coupled modeling and simulation of porous media. Therefore, a complete Solution Verification suite has been developed consisting of analytical solutions for both static and dynamic problems of porous media, in time domain. Verification for fully coupled modeling and simulation of porous media has been performed through comparison of the numerical solutions with the analytical ones. Modeling and simulation is based on the so called, *u–p–U* formulation. Of particular interest are numerical dispersion effects which determine the level of numerical accuracy. These effects are investigated in detail, in an effort to suggest a compromise between numerical error and computational cost.

Keywords: verification; finite elements; fully coupled analysis; porous media; numerical dispersion

1. Introduction

One of the main questions raised when results of a numerical analysis are evaluated is: "How much can (should) we trust model implementations and how much can (should) we trust numerical simulations?" Trust in numerical implementation is gained through a verification process, while, trust in results obtained from numerical simulation, is gained through a validation process (Oberkampf *et al*. 2002, Roy and Oberkampf 2011).

*Corresponding author, Professor, E-mail: jeremic@ucdavis.edu
[a] Ph.D. Student, E-mail: ptasiopoulou@gmail.com
[b] Associate Professor, E-mail: mtaiebat@civil.ubc.ca
[c] Geotechnical Engineer, E-mail: ntafazzoli@ucdavis.edu

http://www.techno-press.org/?journal=csm&subpage=7 ISSN: 2234-2184 (Print), 2234-2192 (Online)

- **Verification** is a process of determining that a model implementation accurately represents the developer's conceptual description and specification. It is essentially a mathematics issue and it provides evidence that the model is solved correctly.
- **Validation**, on the other hand, is a process of determining the degree to which a model is accurate representation of the real world from the perspective of the intended uses of the model. It is a physics issue, and it provides evidence that the correct model is solved.

Verification and Validation (V&V) are the primary means of assessing accuracy in modeling and computational simulations in order to build confidence and credibility in numerical predictions. Oberkampf *et a*l. (2002) mainly focus on trying to accurately model the "real world", aiming to provide verified and validated computer simulation of the reality. Slightly different approach is taken by Oden *et al*. (2010a,b), where the actual purpose of numerical simulation is to facilitate the engineering decision process, rather than to explicitly represent the "real world". Despite the alternative approaches on the objectives of numerical modeling, it is important to note that both schools of thought place significant emphasis on the need for validation of numerical predictions under uncertainty. In an attempt to describe how V&V provide the connection between reality and numerical simulation (computer implementation) in the process of reaching an engineering decision, a flow chart has been constructed and shown in Fig. 1.

It is evident that Verification and Validation procedures have separate but complementary objectives by definition: i) the model is solved correctly (Verification) and ii) the correct model is solved (Validation). On this basis, they should be dealt as two distinct stages requiring different activities in order to achieve them. In particular, two main activities related to verification procedure can be described as (Oberkampf *et al*. 2002):

- **Code Verification** which identifies and removes errors in computer coding. It can further be separated into: (a) **numerical algorithm verification**, used to ensure that all the numerical algorithms are correctly implemented in the code, and (b) **software quality assurance**, used to ensure that the program system is implemented reliably so that it produces repeatable (stable) results with different compilers and on different computer architectures.
- **Solution Verification** which quantifies numerical errors in computed solutions. Numerical accuracy can only be estimated by direct comparison with analytical solutions for a given application. Thus, evidence that the model can be solved correctly is provided.

On the other hand, Validation procedure involves numerical simulation of realistic conditions and thus, direct comparison with experiments and/or well documented case histories is needed. It is common in practice that only validation procedures are performed, considered misleadingly to show enough evidence that the numerical code is appropriate to solve correctly realistic numerical models, while the verification stage is omitted. Therefore, it should be emphasized that verification is the initial necessary step to ensure that numerical solution of the model is accurate while validation is the final stage to ascertain the numerical model can represent realistic conditions and thus, numerical predictions can be trusted.

The current study focuses on the Verification stage and particularly, on the solution verification procedure, assuming that code verification, which is a strictly programming issue, has been successfully performed. The twofold goal of this paper is to: a) provide a complete solution verification suite for fully coupled, static and dynamic behavior of porous solid-fluid systems, consisting of analytical solutions for porous media in time domain, available in literature, which can be used to verify any finite element/finite difference code and b) to use this particular solution

verification suite in order to verify the UCD Computational Geomechanics Group's implementation of 3D *u–p–U* finite elements (Jeremić *et al*. 2008), which is available through an open source license. The available analytical solutions are provided for idealized problems, based on assumptions such as linear elastic behavior and simplified geometries (mostly 1D). Validation of coupled behavior using elasto-plastic material models, is the subject of another paper Tasiopoulou *et al*. (2014).

It is important to note that this paper provides, to our knowledge, the first verification of fully coupled (porous solid – pore fluid) modeling and simulation. In the past, there were few published papers that used some of the analytical and numerical solutions, used here, for comparison purposes. For example a paper by Gajo *et al.* (1994), published a while ago, focused on comparing different methods, namely *u–p–U*, *u–U* and *u–w* and used two closed form solutions for that purpose. However, they did not provide details of numerical algorithms used, since they used the same algorithm and parameters (whatever they were) comparing different methods (as noted above, *u–p–U*, *u–U* and *u–w*). Focus of this paper is entirely on verification of *u–p–U* method. For this purpose all the available closed form solutions (to our knowledge) are used and all the algorithms and parameters that we used are fully documented. It can be claimed that the *u–p–U* formulation developed by Zienkiewicz and Shiomi (1984), together with our implementation (presented verification, and validation provided by (Tasiopoulou *et al*. 2014)), is now complete.

2. Governing equations of porous media

The response of fully saturated soils under transient loads plays an important role in geotechnical engineering. A literature review on the subject of two-phase materials identifies two major theories which have been developed during the last century and are currently used, namely the Biot theory and the theory of Porous Media. Biot's theory is initially based on the work of Terzaghi (1923), who proposed a model for one-dimensional consolidation. Theory of Porous Media is based on the axioms of continuum theory of mixtures extended by the concept of fractions by Bowen (1980, 1982), Ehlers (1993).

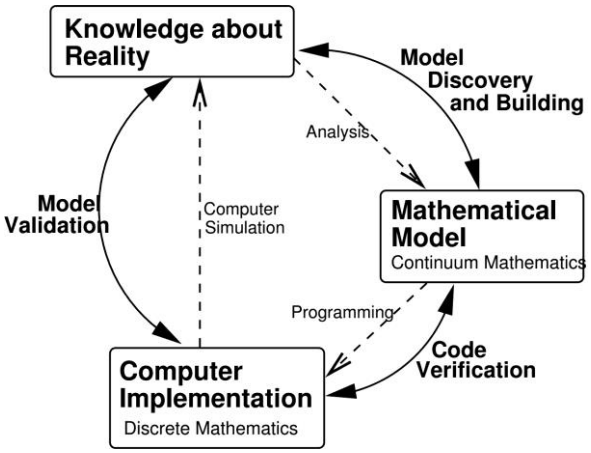

Fig. 1 Schematic representation of the role of Verification and Validation on numerical modeling (inspired from Oberkampf *et al*. 2002, Roy and Oberkampf 2011, Oden *et al*. 2010a)

Biot (1941) presented a theoretical description of linear elastic porous materials fully saturated by a viscous fluid under quasi-static conditions. Extensions of his theory to anisotropic cases (Biot 1955) and to poroviscoelasticity (Biot 1956a,b,c) followed. In Biot's theory a fully saturated material is considered, which consists of two compressible parts: the solid skeleton and the pore fluid. Thus, the solid displacements, $u_i$and the fluid displacements, U_i, are introduced. The equations of motion are formed by stating the balance of momentum, or else the dynamic equilibrium, for the solid skeleton and the pore fluid separately. Zienkiewicz and Shiomi (1984) presented a slightly different formulation, which is based on the concept of Biot's theory; however, it is more convenient for numerical solution. Alternatively to the fluid displacements, a relative displacement of fluid to the solid, w_i (the so-called seepage displacement) is used. Moreover, no additional mass density, $\rho\alpha$, is introduced for the dynamic interaction between the fluid and the skeleton, in contrast to Biot's theory.

Formulation presented by Zienkiewicz and Shiomi (1984) is the most general one and is used in our developments. They did not, however, provide verification of developed formulation that will prove that the formulation is implemented accurately and that the examples are solved correctly. Detailed solution verification of *u–p–U* formulation is precisely the goal of this paper.

Fully coupled (*u–p–U*) formulation is given below in some detail, and is needed as reference for some of the verification solutions given later in the paper. We start from the relationship between effective stress, total stress and pore pressure, written as $\sigma'_{ij} = \sigma_{ij} + \alpha\delta_{ij} p\rho\alpha$, where σ'_{ij} is the effective stress tensor[*], σ_{ij} is total stress tensor, δ_{ij} is Kronecker delta, p is the pore fluid pressure[†]and $\alpha$is the Biot constant that depends on the geometry of material voids. For the most part, in soil mechanics problems, $\alpha \approx 1$ can be assumed, so that the relationship between total and effective stress becomes $\sigma'_{ij} = \sigma_{ij} + \delta_{ij} p$, which corresponds to the classical effective stress definition by Terzaghi (1943).

The material behavior of soil skeleton (porous solid) is fully dependent on the pore fluid pressures. The behavior of pore fluid is assumed to be elastic and thus all the material nonlinearity is concentrated on the soil skeleton. The soil behavior ('mixture' of soil skeleton and pore fluid) can thus be described using single–phase constitutive analysis approach for skeleton combined with the full coupling with pore fluid. The overall equilibrium (momentum balance) equation for the soil-fluid "mixture" can be written as

$$\sigma_{ij,j} = \rho\ddot{u}_i - \rho_f \ddot{w}_i + \rho b_i = 0 \tag{1}$$

where $\ddot{u}_i$is the acceleration of the solid part, b_i is the body force per unit mass, $\ddot{w}_i$ is the fluid acceleration relative to the porous solid. For fully saturated porous media (no air trapped inside), density is equal to $\rho = n\rho_f + (1-n)\rho_s$, where n is the porosity, ρ_s and ρ_f are the soil particle and fluid density, respectively. For the pore fluid, the equation of momentum balance can be written as

$$-p_i - R_i - \rho_f \ddot{u}_i - \frac{\rho_f \ddot{w}_i}{n} + \rho_f b_i = 0 \tag{2}$$

where R is the viscous drag force. According to the Darcy's seepage law, the viscous drag forces R

[*] stresses are positive in tension
[†] pore pressure is positive in compression

between soil matrix and pore fluid can be written as $R_i = k_{ij}^{-1} w_j$, where k_{ij} is the tensor of anisotropic intrinsic permeability coefficients. For simple case of isotropic permeability, scalar value of permeability *k* is used, so as $R_i = k^{-1} w_j$. The permeability *k* used here with dimension of [L^3TM^{-1}] is different from Darcy permeability (hydraulic conductivity), k_D, which has the dimension of velocity, i.e., [LT^{-1}]. Their values are related by $k = k_D / g\rho_f$, where *g* is the gravitational acceleration and ρ_f is the density of the pore fluid.

The final equation is the mass conservation of the fluid flow expressed by

$$\dot{w}_{i,i} + \alpha \dot{\varepsilon}_{ii} + \frac{\ddot{p}}{Q} = 0 \tag{3}$$

where bulk stiffness of the mixture *Q* is expressed as $1/Q = n/K_f + (\alpha - n)/K_s$, and K_s and K_f are the bulk moduli of the solid (particles, not the skeleton) and fluid phases, respectively.

In the above governing equations, convective terms of lower order are omitted. A change of variable is performed by introducing an alternative variable U_i, defined as $U_i = u_i + w_i/n$, that represents absolute displacement of the pore fluid. Thus, the basic set of unknowns comprises the soil skeleton displacements ui, the fluid pore pressure *p*, and the fluid displacements U_i. The set of the modified governing equations is summarized below

$$\sigma'_{ij,j} - (\alpha - n) p_{,i} + (1-n)\rho_s b_i - (1-n)\rho_s \ddot{u}_i + nR_i = 0 \tag{4}$$

$$-np_{,i} + n\rho_f b_i - n\rho_f \ddot{U}_i - nR_i = 0 \tag{5}$$

$$-n\dot{U}_{i,i} = (\alpha - n)\dot{\varepsilon}_{ii} + \frac{1}{Q}\dot{p} \tag{6}$$

From the modified Eqs. (4)-(6), we can see that only $\ddot{u}_i$ occurs in the first equation, and only $\ddot{U}_i$ in the second, thus leading to a convenient diagonal form in discretization.

This theoretical approach describes the interaction of solid skeleton and pore fluid with three major equations, governing both dynamic and quasi–static phenomena: i) equilibrium of total solid-fluid "mixture" – Eqs. (1) and (4), ii) equilibrium of pore fluid – Eqs. (2) and (5), and iii) mass conservation of the fluid flow – Eqs. (3) and (6). The boundary conditions imposed on these variables will complete the problem. These equations together with an appropriate constitutive relationship describe the behavior of solid skeleton accounting for its full interaction with the pore fluid under both quasi-static and dynamic conditions. Herein, the constitutive relationship between increments of effective stress and strain of the solid skeleton is given in a general incremental form

$$d\sigma'_{ij} = D_{ijkl} d\varepsilon_{kl} \tag{7}$$

where $\varepsilon_{ij} = (u_{i,j} + u_{j,i})/2$ is the small strain tensor of the solid skeleton, and D_{ijkl} is the tangent stiffness that can be elastic or elasto-plastic.

The u–p–U formulation considers compressible pore fluid and solid grains. Additionally, due to computation of fluid inertia forces, this formulation is applicable to any range of frequency for

which the hypothesis of constant permeability is valid (Gajo *et al*. 1994). Moreover, the u–p–U formulation resolves the issues of volumetric locking by including the displacements of both the solid skeleton and the pore fluid, and the pore fluid pressure as well. This formulation uses (dependent) unknown field of pore fluid pressures to stabilize the solution of the coupled system. The pore fluid pressures are connected to (dependent on) displacements of pore fluid, as, with known volumetric compressibility of the pore fluid, pressure can be calculated.

An important advantage of u–p–U formulation over commonly used u–p formulations is that velocity proportional viscous damping is introduced directly through the damping tensor which is a function of porosity and permeability of the soil skeleton. This viscous damping provides for physically based, velocity proportional energy dissipation, stemming from the interaction of pore fluid and the porous solid (soil) skeleton. In addition to these advantages, the inclusion of both solid skeleton and pore fluid displacements in the field of unknowns allows for independent treatment of accelerations of both constituents (skeleton and fluid) which improves accuracy of simulations. Some details of the finite element formulation and implementation is given in the appendix for reference.

3. Solution verification suite

Solution verification of the *u–p–U* formulation and its implementation is presented in the following. Analytical solutions for porous media, found in literature, are used to verify numerical solutions obtained by application of the developed code. The analytical solutions in time domain, available in literature, have been developed for linear elastic porous media and simplified geometries (mostly 1D) and they are divided into two main categories, based on: a) consolidation theory, where no inertia effects are taken into account, called quasi-static poroelasticity, and b) dynamic version of the two-phase theory, called poroelastodynamics. Characteristics solutions from both categories are chosen in the following to verify the *u–p–U* finite element formulation, as developed by Jeremic *et al*. (2008).

It should be mentioned that the majority of the analytical solutions are provided for idealized examples, such as 1D linear elastic wave propagation, which are not always representative of realistic cases in terms of 3D geometry and non–linearity. However, while they would seem to be inadequate for Validation purposes, which require realistic experiments and/or well documented case histories (see Tasiopoulou *et al.* (2014) for more details), they successfully serve the mathematical objective of Verification, ensuring the accuracy of the numerical solution provided by the code.

3.1 Quasi–static poroelasticity

This section focuses on analytical solutions based on coupled theory of linear porous media under quasi– static conditions (Coussy 1995, 2004). Eqs. (1) and (2), which are based on equilibrium of total "mixture" and fluid respectively, are reformed in order to apply for quasi–static phenomena (inertia terms are omitted). Thus, Eq. (1) is written as

$$\sigma_{ij,j} = 0 \tag{8}$$

and Eq. (2), assuming isotropic permeability, is written as

$$-p_{,i} - \frac{\dot{w}_i}{k} + \rho_f b_i = 0 \tag{9}$$

Differentiating Eq. (9) with respect to spatial coordinates, we obtain

$$\ddot{w}_{i,i} = -kp_{,ii} \tag{10}$$

Combining Eqs. (10) and (3), the mass conservation equation becomes

$$\alpha\dot{\varepsilon} + \frac{\dot{p}}{Q} = kp_{,ii} \tag{11}$$

A simple linear constitutive relationship between effective stress and strain is considered

$$\sigma_{ij} = \left(K - \frac{2}{3}\mu \right)\varepsilon_v \delta_{ij} + 2\mu\varepsilon_{ij} + \alpha p\delta_{ij} \tag{12}$$

where K is the bulk modulus, μ is the shear modulus, and ε_v is the volumetric strain of porous solid skeleton. Combination of Eqs. (8) and (12), and subsequent differentiation with respect to spatial coordinates, leads to $\left(K + 4\mu/3\right)\varepsilon_{v,ii} - \alpha p_{,ii} = 0$, which can be solved for ε_v as

$$\varepsilon_v = \frac{\alpha p}{K + \left(4/3\right)\mu} \tag{13}$$

Lastly, differentiating ε_v from Eq. (13) with respect to time and substituting it in Eq. (11) in combination with the relationship $K_u = K + \alpha^2 Q$ (where K_u is the undrained bulk modulus of soil), the diffusion equation is derived as

$$\dot{p} = c_f\, p_{,ii} \tag{14}$$

where c_f is the fluid diffusivity coefficient, defined as

$$c_f = kQ\frac{K + \left(4/3\right)\mu}{K_u + \left(4/3\right)\mu} \tag{15}$$

Coussy (1995, 2004) has presented analytical solutions for the diffusion Eq. (14) for different boundary condition problems which have been used as verification examples and are studied in the following.

3.1.1 Vertical Consolidation of a Soil Layer

Analytical Solution by Coussy (2004) – A soil layer of thickness h in the z direction, composed of isotropic, homogeneous and saturated poroelastic material is assumed, as shown in Fig. 2(a). The top surface of the soil layer, $z = 0$, is drained, while its base, $z = h$, is rigid and impervious.

Since this is a one-dimensional problem, the only non-zero displacement is the vertical one, u_z. In particular, the fluid pore pressure, p, as well as the displacement, u_z , depend only on z and t. Thus, the only non-zero strain component is $\varepsilon_{zz} = \partial u_z/\partial z$. The hydraulic boundary conditions require that $p = 0$ for the soil surface ($z = 0$) and $\partial p/\partial z = 0$ for the base of the layer ($z = h$). The undeformability of the substratum requires that the vertical soil displacement, u_z , is zero (u_z = 0

for $z = h$). At time $t = 0$, the instantaneous vertical constant load w is suddenly applied on the top surface $z = 0$. The equilibrium requires that, for $t > 0$ and $z = 0$, $\sigma_{zz} = -\varpi$. Thus, the new fields of fluid pressure and displacement, induced by the external loading, remain to be determined.

Application of the constitutive Eq. (12) gives

$$\frac{\partial u_z}{\partial_z} = \varepsilon_{zz} = \frac{\alpha p - \varpi}{K + (4/3)\mu} \tag{16}$$

The instantaneous response of the porous medium to any external loading is undrained and can be expressed in the form:

$$\varepsilon(t = 0_+) = -\frac{1}{\alpha M} p(t = 0_+) \tag{17}$$

which, when combined with Eq. (12), leads to

$$p(z, t = 0_+) = \frac{\alpha M \varpi}{K_u + (4/3)\mu} \frac{\partial d_z}{\partial_z}(z, t = 0_+) = \varepsilon_{zz} = \frac{-\varpi}{K_u + (4/3)\mu} \tag{18}$$

Finally, in case of one-dimensional consolidation, the diffusion Eq. (14), needed to be solved, reads:

$$t > 0 \qquad \frac{\partial p}{\partial t} = c_f \frac{\partial^2 p}{\partial_z^{\,2}} \tag{19}$$

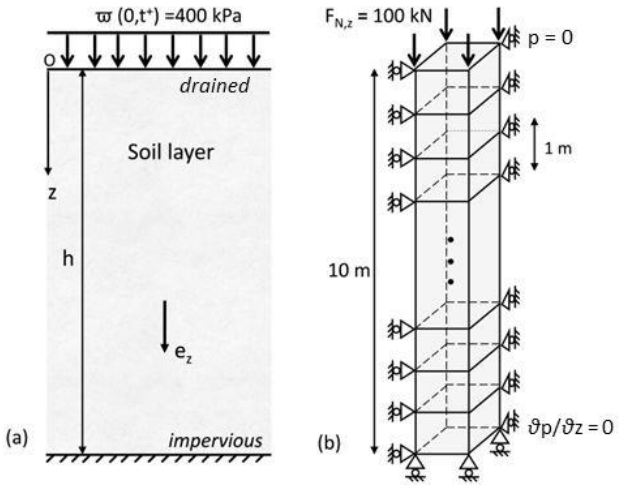

Fig. 2 (a) The geometry of the soil layer of thickness h under uniform constant vertical pressure $\varpi = 400$ kPa applied at the surface, and (b) the finite element mesh with the appropriate boundary conditions and loading at top

Satisfying the above mentioned boundary conditions, the fluid pressure can be expressed in the form of infinite series

$$p(z,t) = \frac{\alpha M \varpi}{K_u + (4/3)\mu} \sum_{m=0}^{\infty} \frac{4}{\pi(2m+1)} \mathrm{Sin}\left(\frac{(2m+1)\pi}{2}\frac{z}{h}\right) \exp\left(-\frac{(2m+1)^2\pi^2}{4}\frac{t}{\tau}\right) \tag{20}$$

Each term of the series decreases exponentially with respect to the ratio t/τ, with τ being the characteristic consolidation time, defined as

$$\tau = \frac{h^2}{c_f} \tag{21}$$

By substituting Eq. (20) into Eq. (16), the series converges and, after integration term by term, we obtain

$$\begin{aligned} u_z(z,t) &= \frac{\varpi(h-z)}{K + (4/3)\mu} + \left(\frac{\varpi h}{K_u + (4/3)\mu} - \frac{\varpi h}{K + (4/3)\mu}\right) \\ &\sum_{m=0}^{\infty} \frac{8}{\pi^2(2m+1)^2} \cos\left(\frac{(2m+1)\pi}{2}\frac{z}{h}\right) \exp\left(-\frac{(2\mathrm{m}+1)^2\pi^2}{4}\frac{t}{\tau}\right) \end{aligned} \tag{22}$$

Using Eq. (22) and substitute z = 0, the total settlement of the soil layer, s, can be expressed as

$$s(t) = s_\infty + (s_{0+} - s_\infty) \sum_{m=0}^{\infty} \frac{8}{\pi^2(2m+1)^2} \exp\left(-\frac{(2m+1)^2\pi^2}{4}\frac{t}{\tau}\right) \tag{23}$$

where

$$s_{0+} = \frac{h\varpi}{K_u + (4/3)\mu} \; ; \; s_\infty = \frac{h\varpi}{K + (4/3)\mu} \tag{24}$$

Numerical Analysis – A soil column of u–p–U, 8-node brick, finite elements is used to model the horizontal layer. Each element has dimensions 1 m×1 m×1 m, resulting in soil–column mesh, 10 m high, as illustrated in Fig. 2(b). The elastic material properties, shown in Table 1, are chosen as indicative values for the natural soil deposit. A constant uniform vertical pressure of 400 kPa is instantaneously applied on the top of the finite element mesh.

The following boundary conditions are applied to the model, shown in Fig. 2(b): the solid and fluid displacements are fixed at the base and the pore pressure is kept zero at the top surface. In order to simulate the 1D consolidation problem, the lateral movement of the solid and fluid phase is suppressed so that the vertical displacement remains the only non-zero displacement. To remedy any artificial oscillation due to spatial and time discretization, numerical damping is introduced into the analysis by using $\gamma = 0.6$ and $\beta = 0.3025$ for the Newmark time integrator (Newmark 1959; Argyris and Mlejnek 1991).

The instantaneous response of the soil skeleton is undrained which leads to sudden increase of pore pressure. The boundary condition of perfect drainage at the surface ($p = 0$) causes an upward flow of the pore water, so that pore pressure gradually reduces with time, as depicted by Fig. 3(a). The time factor, T_v is defined as $T_v = t/\tau$ so that for $T_v = 1$, the process of consolidation is

considered to have been completed, since the rate of dissipation has been practically diminished. Fig. 3(b) depicts the distribution of pore pressure with depth for different moments in time, T_v, confirming the upward movement of pore water, as the rate of pore pressure dissipation is clearly greater for depths closer to the surface. The gradual upward movement of pore water leads to increase of the vertical soil displacement with time, as shown in Fig. 4(a). It can be concluded that the numerical analysis can effectively demonstrate the process of the dissipation of the pore pressure in agreement with the analytical solution by Coussy (2004). Moreover, the numerical analysis based on u–p–U formulation permits the calculation of upward fluid movement, U_z, plotted with time in Fig. 4(b). The upward displacement of the fluid, U_z, at the end of consolidation has been computed as 0.39 m, more than the final downward displacement of the soil skeleton (0.33 m). Thus, an accurate estimation of the change in porosity due to settlement of the soil and consequent upward drainage of amount of pore fluid can be performed. The amount of fluid that escaped is calculated as $\Delta V_f = nU_z = 0.46 \times 0.39$ m $\times$ 1 m $\times$ 1 m = 0.1794 m^3. The change of solid-skeleton volume is equal to $\Delta V_s = (1 - n)Us = 0.54 \times 0.33$ m $\times$ 1 m $\times$ 1 m = 0.1782 m^3. If the total initial volume of soil is V = 10 m^3 and the initial volume of pore fluid is nV = 4.6 m^3, the final porosity at the end of consolidation is estimated $n' = (4.6 - 0.1794)/(10 - 0.1782) = 0.45$, less than the initial one, n = 0.46, indicating slight compaction of the soil layer.

Table 1 Soil properties used in numerical analysis of quasi–static problems

Parameter	Symbol [Units]	1D consolidation	Line Injection
Gravity acceleration	g [m/s^2]	9.81	9.81
Soil Young's modulus	E [kN/m^2]	10^4	1.2 x 10^6
Soil Poisson's ratio	v	0.25	0.2
Solid density	ρ_s [ton/m^3]	2.65	2.7
Fluid density	ρ_f [ton/m^3]	1.0	2.7
Solid bulk modulus	K_s [kN/m^2]	37 x 10^6	3.6 x 10^7
Fluid bulk modulus	K_f [kN/m^2]	2.2 x 10^6	1.0 x 10^{17}
Porosity	n	0.46	0.4
Biot coefficient	α	1.0	1.0
Darcy permeability	k_D [m/s]	10^{-3}	3.6 x 10^{-6}
Soil drained bulk modulus	K [kN/m^2]	6.67 x 10^3	6.7 x 10^5
Soil undrained bulk modulus	K_u [kN/m^2]	4 x 10^6	6.0 x 10^7
Fluid diffusivity coefficient	c_f [m^2/s]	1.2	0.5

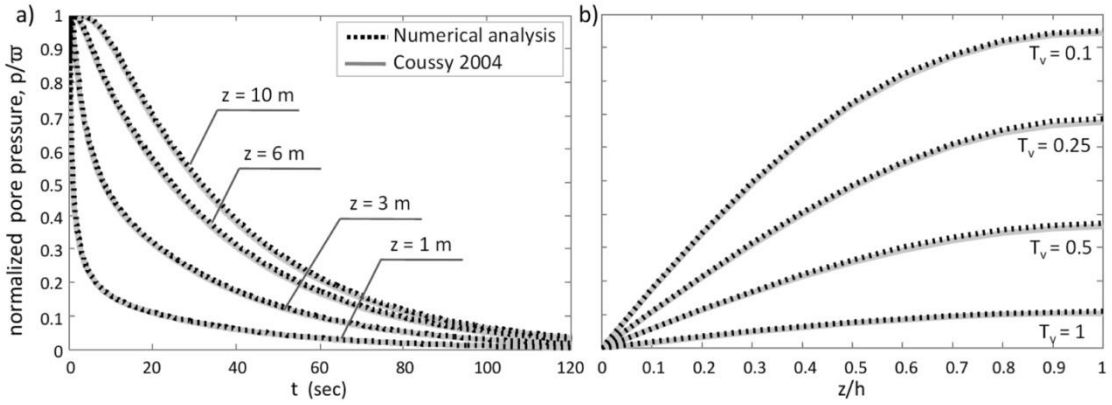

Fig. 3 Comparison between numerical analysis and analytical solution by Coussy (2004): (a) normalized pore pressure at various depths with respect to real time, *t*, and (b) distribution of normalized pore pressure with normalized depth, z/h, for different time factors, T_v

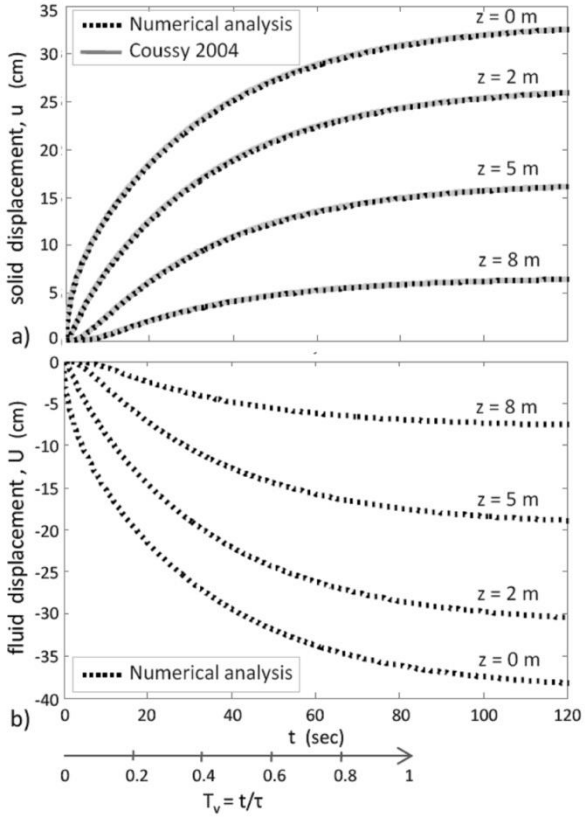

Fig. 4 (a) Comparison between numerical analysis and analytical solution by Coussy (2004) in terms of time histories: (a) solid–skeleton displacements, and (b) fluid displacements, for various depths

3.1.2 Line injection of fluid in a reservoir

Analytical Solution by Coussy (2004) – A reservoir of infinite extent composed of an isotropic, homogeneous and saturated poroelastic material is considered. Through a cylindrical well of negligible dimensions, fluid mass injection is performed in all directions orthogonal to the well axis of symmetry, forming the z axis of coordinates. The flow rate of fluid mass injection is constant and equal to q. This is a problem of cylindrical symmetry, requiring the use of cylindrical coordinates (r,θ,z). The vectors of relative flow of fluid mass, $\boldsymbol{w}$, and solid–skeleton displacement, $\boldsymbol{\xi}$ are expressed as $\boldsymbol{w} = w(r, t)\boldsymbol{e_r}$ and $\boldsymbol{\xi} = \xi(r, t)\boldsymbol{e_r}$, where $\boldsymbol{e_r}$ is the unit vector along the radius. Solid–skeleton strain components are derived in the form

$$\varepsilon_{rr} = \frac{\partial \xi}{\partial r} \; ; \; \varepsilon_{\theta\theta} = \frac{\xi}{r} \text{ and } \varepsilon_{ij} = 0 \tag{25}$$

Thus, Eqs. (13) and (14) are reformed in cylindrical coordinates

$$\varepsilon_v = \frac{1}{r}\frac{\partial(r\xi)}{\partial r} = \frac{\alpha p}{K + (4/3)\mu} \tag{26}$$

$$\frac{\partial p}{\partial t} = c_f \left(\frac{1}{r}\right)\frac{\partial}{\partial r}\left(\frac{r\partial p}{\partial r}\right) \tag{27}$$

Requiring that the fluid flow reduces to zero infinitely far from the well, $rw \rightarrow 0$ as $r \rightarrow \infty$, the fluid mass balance relationship is applied

$$\int_0^\infty \dot{w}_{,r}(r,t)\, 2\pi r dr = q \tag{28}$$

The solution of the set of Eqs. (26)-(28), and (3) for the instantaneous injection of a finite volume of fluid, Ω, is given in the following form

$$p = Q\frac{K + (4/3)\mu}{K + u + (4/3)\mu}\frac{\Omega}{4\pi c_f t}\exp\left(-\frac{r^2}{4c_f t}\right); \xi = \frac{\alpha Q\Omega}{2\pi r(K_u + (4/3)\mu)}\left[1 - \exp\left(-\frac{r^2}{4c_f t}\right)\right] \tag{29}$$

Numerical Analysis – As a result of axis symmetry of the geometry, the model has been developed for $\pi/2$ segment, 5 cm thick, with radius equal to 1 m. A cylindrical well is drilled at the center of the model, with 1 cm radius, having negligible size when compared to the model radius, but still providing well–shaped elements. Due to plane–strain conditions, all the movements for solid and fluid phases are suppressed along the vertical axis of symmetry, z. The u and U nodes along the outside perimeter are fixed. It should be noted that Ω is the volume of the fluid injected per unit of vertical well length, m^3/m. In order to generate the volume of 1 cm^3/m, the corresponding fluid displacement of the nodes along the well has been calculated and applied as a step function at the time $t = 0$ sec. For simplicity, the initial fluid pressure p_0 is set to be 0 kPa. The analytical solution is studied below using the set of parameters shown in Table 1.

In the analysis, the pore pressure and the radial displacements are recorded at three points on the radius (10 cm, 50 cm, and 85 cm). The analytical and numerical results compare well with each other as indicated by Fig. 5. The time step, Δt, was set equal to 1 sec; thus, the first data point is recorded at the time of 1 sec.

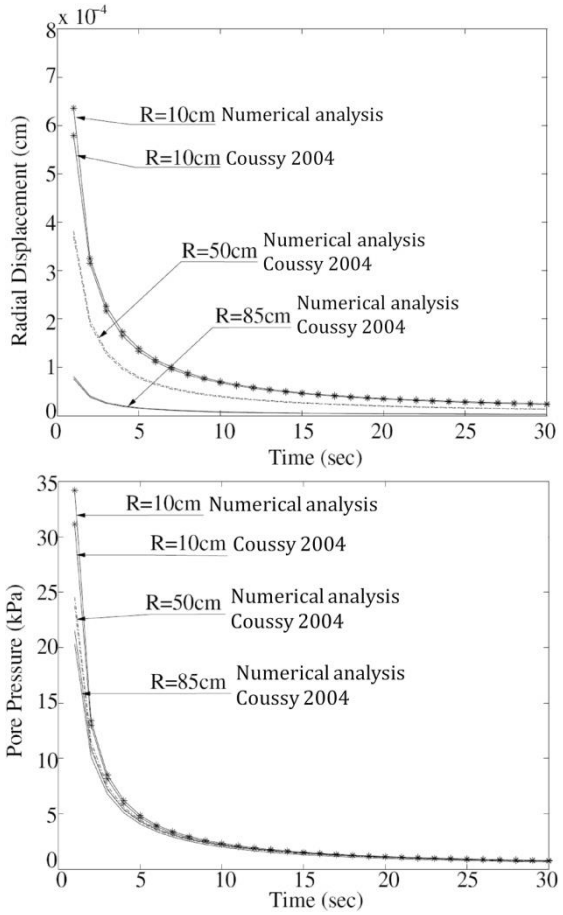

Fig. 5 Comparison between numerical analysis and analytical solution by Coussy (2004): (a) radial displacement, and (b) pore pressure versus time at different distances, *R*, from the center of the model

3.2 Poroelastodynamics

One of the significant findings by Biot (1956a,b,c) was the identification of two kinds of compressional waves and one shear wave, which has been the starting point for further research on the mechanics of dispersive waves through analytical or numerical approaches. Several analytical and semi-analytical solutions for dynamic poroelasticity are available in the literature, varying with geometry, type of loading, time domain or transformed domain solution, assumptions related to the compressibility of the fluid and the formulation used (u–p, u–p–U , u–U). A review of this wide range of solutions in dynamic poroelasticity is nicely presented by Schanz (2009). The current paper focuses on solutions regarding one-dimensional wave propagation in saturated linear elastic porous media due to step and sinusoidal excitations.

In order to study the accuracy of u–p–U finite element procedure in representing a dispersive wave propagation in saturated soil, numerical dispersion effects should be taken into account. Dependence of the wave-velocity on the frequency content of the excitation is the basic concept behind the theory of dispersive waves. Thus, when wave propagation is modeled in a numerical scheme, numerical features, such as the element size, integration scheme, numerical damping, element type etc., should be chosen appropriately, so that the frequency range of the excitation will be represented in the model. Otherwise, the wave-velocities developed in the numerical model will diverge from the theoretical solution due to an artificial dispersion attributed to numerics and not physics (numerical dispersion).

Various theoretical works concern the effect of numerical dispersion (Deraemaeker and Babuska 1999, Hughes 1987, Ihlenburg and Babuska 1995, Semblat and Brioist 2000), highlighting spatial discretization as one of the most influential numerical features. In particular, the effect of numerical dispersion decreases with the increase in wave length, λ, and increases with the increase in mesh size Δh, which can lead to the necessity to use fine meshes, even uneconomical ones for small wave lengths (Deraemaeker and Babuska 1999). A common rule of thumb for typical finite element procedures is to resolve the wavelength by 10 elements (Ihlenburg and Babuska 1995, Hughes 1987); thus the element size, Δh, should be less that 1/10 of the smallest wavelength (λ_{min}) involved in the application

$$\Delta h \leq \frac{\lambda_{min}}{10} \ \textit{where} \ \lambda_{min} = \frac{V_{min}}{f_{max}} \tag{30}$$

where V_{min} is the lowest wave velocity of interest in the simulation and generally, it is a function of the elastic modulus of the medium, while f_{max} is the maximum frequency that is modeled.

Spatial and temporal discretization are linked in a way requiring that mesh spacing is accompanied by an appropriate time interval. As a wave front progresses in space it reaches one point after the other. If the time step in the finite element analysis is too large, the wave front can appear to reach two consecutive nodes at the same moment. This would violate a fundamental property of wave propagation and can lead to instability. In order to ensure that the propagation of wave can be modeled properly, the required time step, Δt, must be limited to

$$\Delta t \leq \frac{\Delta h}{V_{max}} \tag{31}$$

where V_{max} is the highest wave velocity involved, usually being a function of the undrained elastic modulus in case of fully saturated porous media.

3.2.1 Step displacement excitation

Analytical Solution by Gajo and Mongiovi (1995) – An one-dimensional analytical solution of the Biot's equations (using u–U field displacements) is provided by Gajo and Mongiovi (1995) for a general transient problem in poroelasticity. The analytical solution was obtained using Fourier series expansion and it is not based on any assumptions with respect to the inertial, viscous or mechanical coupling. Furthermore, it is applicable to any type of boundary-initial value problem.

Since each term of the Fourier series represents a frequency component of the excitation signal, the analytical solution can describe the behavior of every single frequency component related to the problem. Thus, it can illustrate the mechanics of dispersive wave propagation in which higher

frequencies propagate with two waves and lower frequencies with only one wave,as a function of permeability and travel length. Considering the above, the analytical solution can provide a useful comparative tool towards the verification of the existing numerical solutions based on the finite element method (Gajo *et al*. 1994).

Gajo and Mongiovi (1995) present the response of the porous medium only relative to the first arrival of the waves of the first and second kind. Specifically, analytical results are shown for a finite soil column subjected to a step displacement boundary condition (Heaviside function) at the surface applied both to solid and fluid phases, as shown in Fig. 6(a). This problem can demonstrate better the mechanics of dispersive wave propagation, since the step excitation contains waves of all frequencies. In the following section (3.2.2), analytical solution is compared with numerical analysis for a soil column subjected to a single sine pulse with characteristic predominant frequency of 10^6 Hz, producing smoother wavefronts.

Numerical Analysis – Fine spatial discretization is required due to step boundary condition. This kind of excitation contains waves of all frequencies leading to meshes with a large number of finite elements, according to Eq. (30), which suggests that the appropriate element size is inversely proportional to the maximum frequency introduced to the model. In fact, there is no element size that could satisfy the equation; thus, numerical dispersion is inevitable. It can only be diminished by increasing the spatial refinement. Evidently, a compromise needs to be made between the quantity of numerical error and the computational cost.

Numerical models with three different values of permeability – resulting in three different viscous coupling scenarios ($k = 10^{-8}$ cm3s/g, $k = 10^{-6}$ cm3s/g, $k = 10^{-5}$ cm3s/g) – were solved in order to verify the u–p–U formulation in a wide range of drag forces. At the top surface of the model, a vertical step displacement of 1.0×10^{-3} cm is applied both to the solid and the fluid phases. No lateral flow or displacement is allowed. The base of the model is rigid and impervious, as schematically illustrated in Fig. 6(a).

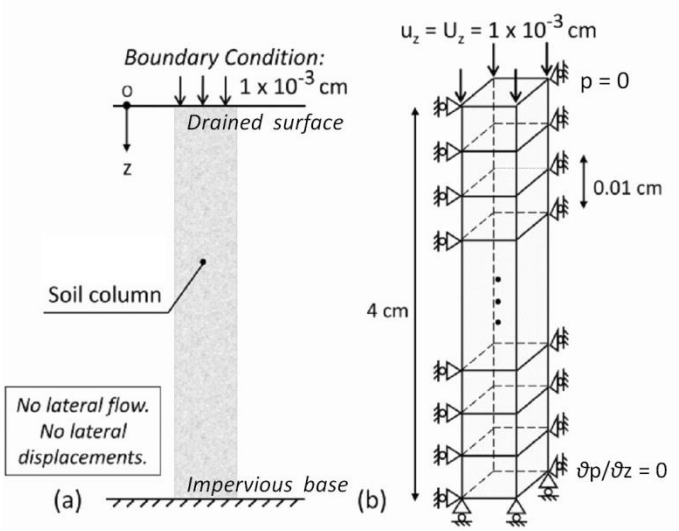

Fig. 6 (a) A representative soil column subjected to a step vertical displacement equal to 1.0×10^{-3} cm at the surface, and (b) the finite element mesh and the applied boundary conditions used for numeric modeling

Table 2 Soil Properties for 1D wave propagation due to various boundary conditions and loading

Parameter	Symbols [Units]	Step/Sine pulse disp. (Gajo and Mongiovi 1995)	Step/Sine loading (de Boer *et al*. 1993)	Step vel. (Hiremath *et al*. 1988)
Gravity acceleration	g [m/s^2]	9.81	9.81	9.81
Soil Young's modulus	E [kN/m^2]	1.2 x 10^6	20 x 10^3	23.2 x 10^6
Soil Poisson's ratio	v	0.3	0.2	0.17
Solid density	ρ_s [ton/m^3]	2.7	2.0	2.66
Fluid density	ρ_f [ton/m^3]	1.0	1.0	1.0
Solid bulk modulus	K_s [kN/m^2]	36 x 10^6	36 x 10^6	36 x 10^6
Fluid bulk modulus	K_f [kN/m^2]	2.2 x 10^6	2.2 x 10^6	2.2 x 10^6
Porosity	n	0.4	0.33	0.18
Biot coefficient	α	1.0	1.0	0.677

According to Gajo (1995), the two extreme values of wave velocity for longitudinal propagation in a porous medium with properties shown in the third column of Table 2, are: V_{min} = 610 m/s and V_{max} = 1819 m/s, corresponding to the case of significantly low viscous coupling, where two longitudinal waves exist (one slow and one fast).

For infinitely large viscous coupling, the velocity of the single longitudinal wave is 1773 m/s. The chosen finite element mesh consists of 400 u–p–U brick finite elements of dimensions 0.01 cm × 0.01 cm × 0.01 cm, creating a soil column 4 cm high, as illustrated in Fig. 6(b). The maximum frequency allowed to be present in a model with the above-mentioned grid spacing is 18.19 × 10^6 Hz for the first longitudinal wave (fast) and 6.1 × 10^6 Hz for the second one (slow). There is a cut-off of greater frequencies imposed by the specific computational mesh.

The maximum time step is equal to (0.0001 m)/(1819 m/s) = 5.5×10^{-8} sec, as suggested by Eq. (31).The selected temporal integration involves 800 steps of Δt = 2.0 × 10^{-8} sec, which allows a maximum wave velocity of 5.0 × 10^5 m/s.

Fig. 7 shows the comparative results for all three different values of viscous coupling using Newmark parameters: γ = 0.6 and β = 0.3025, which introduce numerical damping in the model. In general, the numerical results are in good agreement with analytical solution for 1D wave propagation in fully saturated, elastic porous media. For example, numerical analysis demonstrates that during the propagation of the first wave, the solid and fluid displacement are in phase with each other, whereas during the propagation of second wave, the displacements are in opposite phase. In case of high viscous coupling, only one longitudinal wave exists, since the relative motion between solid and fluid phase is highly constrained.

However, as expected, the rise time of wave fronts obtained from the numerical analysis is larger than the rise time estimated by the analytical solution, due to numerical dispersion, observed also by Gajo *et al*. (1994) and Simon *et al*. (1984). This discrepancy is smaller for high viscous coupling which physically induces a more dispersive response, in contrast to low viscous coupling which

produces abrupt wavefronts. This dispersive response in case of large viscous coupling is attributed to the physically based, high viscous damping due to coupling of pore fluid and porous solid, which can be captured by the u–p–U formulation (see matrices C_1, C_2, and $C_3$of Eq. (37), in the appendix).

Furthermore, the rise time of the second wave is even larger; a fact that can be partly attributed to the diffusive behavior of the second wave in low–frequency range. In general, the distortion and the smearing of the wave fronts is a drawback of all types of numerical solutions, which is linked to the limitation of the highest frequency allowed by the computational grid and the numerical damping introduced to the model.

In order to further examine the sensitivity of the numerical solution to characteristic numerical features, such as a) spatial refinement and b) numerical damping, an indicative parametric investigation was conducted. For this purpose, a finer spatial discretization of Δh = 0.005 cm was selected, accompanied by a smaller time step equal to 10^{-8} sec. Two different sets of parameters for Newmark integrator wereused: i) γ = 0.5 and β = 0.25 corresponding to no numerical damping and ii) γ = 0.6 and β = 0.3025, which introduce numerical damping. Fig. 8 shows the numerical response versus the analytical solution for two combinations of spatial and temporal refinement when no numerical damping is introduced in the model (γ = 0.5 and β = 0.25). High-frequency artificial oscillations develop within the model at the first wave arrival with gradually decreasing amplitude over time. Evidently, the oscillations are narrower with equal or smaller amplitude in case of the finer mesh, while the rise time of abrupt wavefronts diminishes, better approaching the analytical solution.

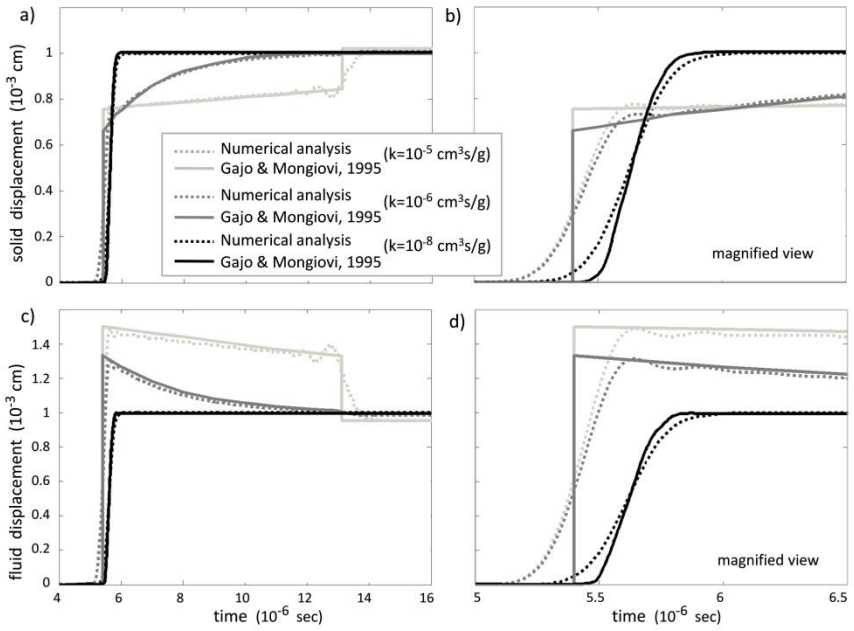

Fig. 7 Comparison between numerical analysis and analytical solution by Gajo and Mongiovi (1995) for three different values of viscous coupling, *k*: (a) solid displacement versus time from 4–16×10^{-6} sec, (b) solid displacement versus time from 5–6.5×10^{-6} sec, (c) fluid displacement versus time from 4-16×10^{-6} sec, and (d) fluid displacement versus time from 5–6.5×10^{-6} sec, obtained 1 cm below the surface

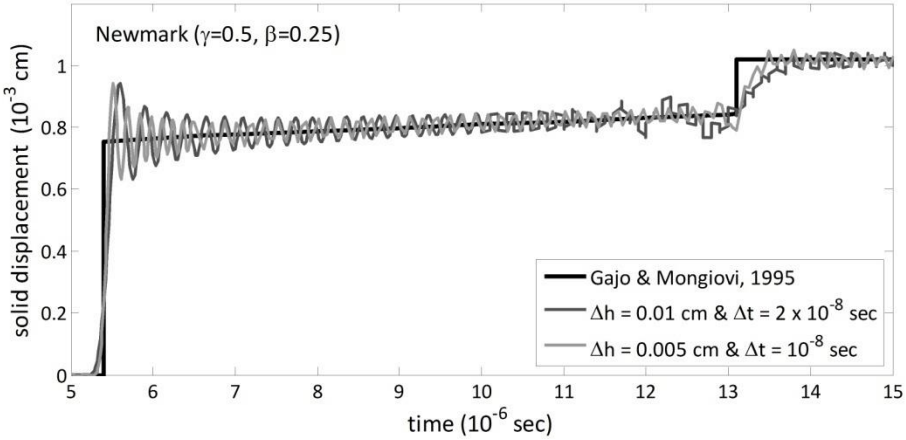

Fig. 8 Analytical solution by Gajo and Mongiovi (1995) versus numerical analysis with no numerical damping (γ = 0.5 and β = 0.25) for two different combinations of spatial and temporal discretization: i) Δh = 0.01 cm and $\Delta t = 2 \times 10^{-8}$ sec, ii) Δh = 0.005 cm and $\Delta t = 10^{-8}$ sec, in the case of viscous coupling $k = 10^{-5}$ cm^{3}s/g

Fig. 9 shows the comparison of numerical results with analytical solution for the two selected meshes when numerical damping is used in the numerical scheme (γ = 0.6 and β = 0.3025). Once more, closer convergence with analytical solution is achieved in case of finer mesh. It is interesting to notice that the slight oscillations occurring close to the wavefronts in case of coarser mesh, have been completely damped out by numerical damping in case of finer spatial discretization. This fact leads to the conclusion that numerical damping is, in this case, more effective in damping out higher-frequency oscillations which develop in case of finer mesh.

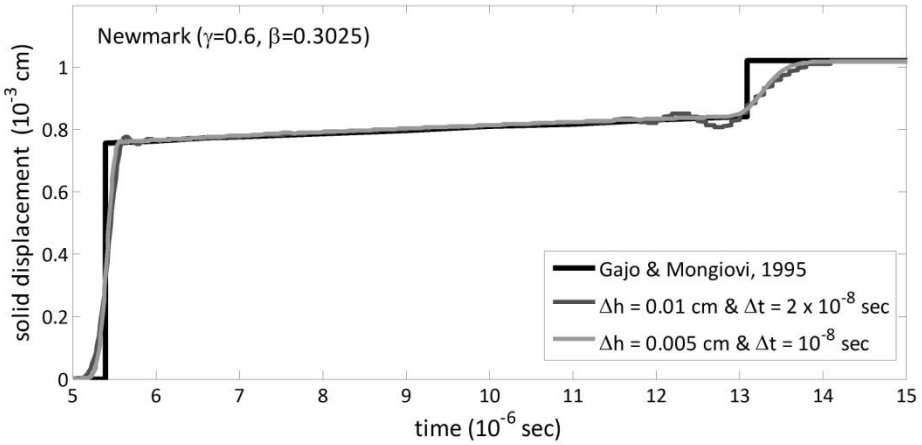

Fig. 9 Analytical solution by Gajo and Mongiovi (1995) versus numerical analysis with no numerical damping (γ = 0.6 and β = 0.3025) for two different combinations of spatial and temporal discretization: i) Δh = 0.01 cm and $\Delta t = 2x10^{-8}$ sec, ii) Δh = 0.005 cm and $\Delta t = 10^{-8}$ sec, in the case of viscous coupling $k = 10^{-5}$ cm^{3}s/g

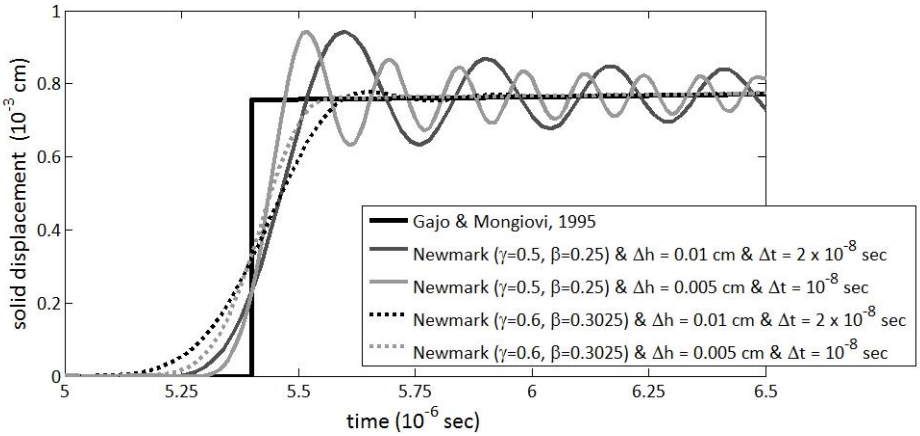

Fig. 10 Analytical solution by Gajo and Mongiovi (1995) versus numerical analysis for two cases of numerical damping: (a) $\gamma = 0.5$ and $\beta = 0.25$ (no numerical damping) and (b) $\gamma = 0.6$ and $\beta = 0.3025$ and for two different combinations of spatial and temporal discretization: i) $\Delta h = 0.01$ cm and $\Delta t = 2 \times 10^{-8}$ sec, ii) $\Delta h = 0.005$ cm and $\Delta t = 10^{-8}$ sec, in case of viscous coupling $k = 10^{-5}$ cm^{3}s/g. Magnified view of the first wavefront

Overall, Fig. 10 suggests that the analytical solution is better approached in terms of the rise time of wavefronts, when no numerical damping is introduced in the model and finer mesh is used. However, numerical damping is needed to damp out the artificial oscillations developed due to the discretization of continuum into finite element model in combination with the range of frequencies imposed by the excitation. The compromise in choosing the parameters of the numerical features is directly related to the desired level of accuracy in capturing the details of response, where both low and high frequency waves are present.

3.2.2 Single sine pulse displacement

In order to investigate the efficiency of u–p–U finite element under more realistic excitations with a characteristic predominant frequency, a single sine pulse displacement was imposed to both solid and fluid phases at the top of a finite soil column. The characteristic duration of the single sine pulse is 10^{-6} sec, corresponding to a predominant frequency of 10^6 Hz. The soil properties assigned to the model are the same as in the previous example and are shown in the third column of Table 2. The minimum wavelength, λ_{min}, is estimated as V_{min}/f_{max} = (610 m/s)/(10^6 Hz) = 6.1×10^{-4} m. According to Eq. (30), the element size is limited to 1/10 of the minimum wavelength, so that it is less than 6.1 × 10−5 m. The selected mesh is comprised of 800 u–p–U brick finite elements of dimensions 0.005 cm × 0.005 cm × 0.005 cm, creating a soil column 4 cm high. The time step is limited to $\Delta t \leq \Delta h/V_{max} = 2.7 \times 10^{-}8$ sec according to Eq. (31). The chosen temporal discretization consists of time intervals equal to $\Delta t = 2 \times 10^{-8}$ sec. Numerical models with three different values of permeability, resulting in three different viscous coupling cases ($k = 10^{-8}$ cm^{3}s/g, $k = 5 \times 10^{-8}$ cm^{3}s/g, and $k = 10^{-5}$ cm^{3}s/g), were analyzed.

Fig. 11 shows the comparative results for all three different values of viscous coupling using New- mark parameters: $\gamma = 0.5$ and $\beta = 0.25$, introducing no numerical damping. In general, the

numerical results converge well with analytical solution, especially for higher values of viscous coupling where the response is physically more dispersive. One can observe that the there is a slight discrepancy between analytical and numerical response in terms of the rise time at the arrival of the pulse, for cases of lower viscous coupling. This fact emphasizes the sensitivity of the response to the spatial refinement even under smoother excitations with a predominant characteristic frequency, particularly for cases of low viscous coupling. The numerical error can be eliminated with finer mesh, as shown in the previous case. However, herein, the effect of numerical dispersion is significantly smaller compared to the example of step excitation and it could be suppressed in case of completely smooth pulse (e.g., Ricker). Moreover, no need for numerical damping occurred since no high frequency artificial oscillations developed as in case of step pulse.

3.2.3 Step loading

Analytical Solution by de Boer *et al*. (1993) – An analytical solution for one-dimensional wave propagation in fluid-saturated elastic porous media is provided by de Boer *et al*. (1993), based on theory of mixtures (Bowen 1980, 1982, Ehlers 1993). The fluid-saturated porous material is assumed to be a two phase system composed of incompressible solid and fluid phases. An exact analytical solution is obtained via Laplace transform technique exhibiting only one independent compressive wave in both the solid and fluid phases, as a result of the incompressibility constraint.

The problem configuration consists of an infinitely long column, extracted from the half-space of a fluid-saturated porous elastic skeleton material. The motions of both solid and fluid materials are constrained to occur only in the vertical direction. Loading is applied to the surface boundary, as a function of time, $\sigma(z = 0, t) = f(t)$. Both solid and fluid displacements, as well as solid skeleton extra stress and pore pressure are obtained with respect to time and depth (de Boer *et al*. 1993). The analytical solution has been developed for i) sinusoidal, ii) step (presented here) and iii) impulsive loading.

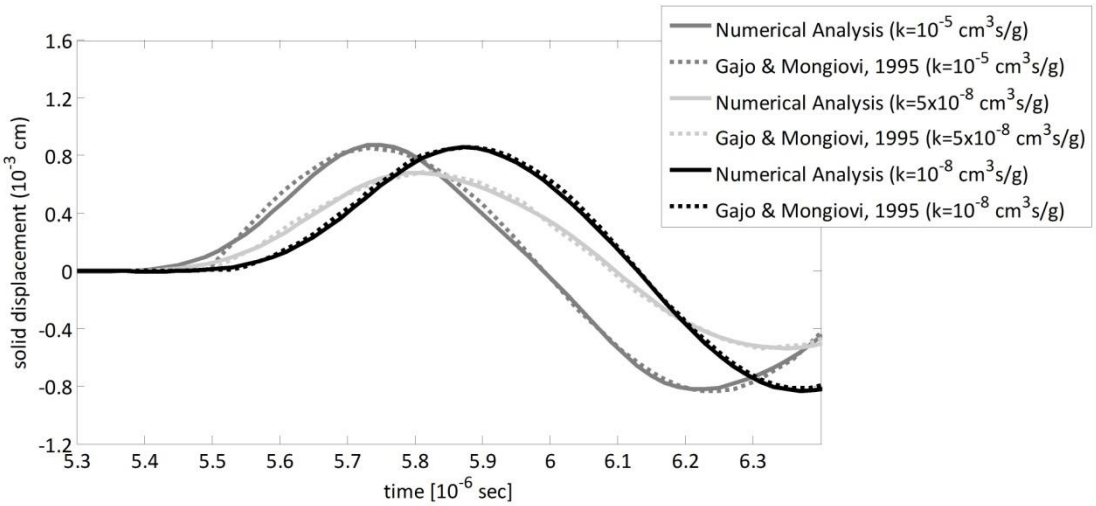

Fig. 11 Comparison between numerical analysis and analytical solution by Gajo and Mongiovi (1995) in terms of solid displacement, obtained 1 m below the surface, for three different values of viscous coupling, *k*

Numerical Analysis – Numerical example for the step loading case was used to verify the implementation of *u–p–U* formulation. Step loading excitation contains all frequencies, thus requiring a fine spatial discretization. However, this example does not examine the details of wavefront; it rather focuses on the long term response describing the consolidation process under dynamic loading. Considering the above, the numerical grid used for the simulation of the 1D shock wave propagation consists of 1000 *u–p–U* brick finite elements of dimensions 1 cm × 1 cm × 1 cm creating a soil column 10 m high. Since the numerical simulation of a semi-infinite soil column is not possible, a soil column of finite depth of 10 m was considered adequate for the current problem configuration. No lateral flow or displacement is allowed in the model; thus, only the vertical displacement is free. The pore pressure is constrained at the top surface to be equal to the atmospheric pressure; thus, modeling drained condition. The base of the model is rigid and impervious.

Table 2 shows the soil properties of the numerical model, which are the same with those used for the analytical results presented in the paper by de Boer *et al*. (1993). The only difference is associated with the elastic modulus, which was selected to be 20 MN/m^2 for the numerical solution instead of 30 MN/m^2, as noted by de Boer *et al*. (1993). The value of Darcy permeability assigned to the soil skeleton is equal to 0.01 m/s. The numerical analysis indicates that the analytical results presented in the paper correspond to a soil column with elastic modulus equal to 20 MN/m^2 instead of 30 MN/m^2. Moreover, it should be mentioned that the solid and fluid (water) compressibility were given realistic values (see the fourth column of Table 2), which practically means that the two constituents can be assumed fairly incompressible compared to the soil–skeleton compressibility.

At the top surface of the soil column, a step loading of $\sigma(z = 0, t) = 3$ kN/m^2 is applied to the solid part through four nodal loads at the top. The nodal loads are developed as

$$F_N(z=0,t) = \frac{\sigma(z=0,t)\times A}{4} = \frac{3\,\mathrm{kN/m^2}\times 0.01\,\mathrm{m}\times 0.01\,\mathrm{m}}{4} = 7.5\times 10^{-5}\ \mathrm{kN} \tag{32}$$

The maximum wave velocity of the soil can be given approximately by equation

$$V_{\max} = \sqrt{\frac{M + aQ}{(1-n)\rho_s + n\rho_f}} = 2000\ \mathrm{m/s} \tag{33}$$

where M is the constrained modulus of the solid skeleton, α is Biot coefficient, while Q is the bulk stiffness of a mixture, defined after Eq. (3). Thus, according to Eq. (31) the time step should be 5×10^{-6} sec or less. The selected temporal integration involves 80000 steps of $\Delta t = 5.0\times10^{-6}$ sec. The Newmark parameters used in the analysis are: $\gamma = 0.7$ and $\beta = 0.4$. This sets of parameters introduce considerable numerical damping to the model which can increase numerical dispersion, but as mentioned before, the current study does not focuses on the details of the high frequency components which are quickly damped out with time. Figs. 12-14 show the comparison between analytical and numerical results.

In general, the numerical results are in good agreement, with respect to time and depth, with those obtained by the analytical solution. During the consolidation process, the solid skeleton settles and the fluid escapes out of the solid skeleton while the load is transferred from the pore pressure to the solid skeleton stress. The only discrepancy between analytical and numerical results is found in the pore pressures which develop an oscillatory trend in case of numerical analysis. The existence of oscillatory waves has also been observed and discussed by Zienkiewicz and Shiomi (1984). These artificial oscillations, attributed to the combination of numerical features and the nature of dynamic

step loading, are damped out over time. Numerical damping would be more efficient in eliminating the artificial oscillations if finer mesh was used and thus, higher-frequency oscillations were developed. This conclusion, indicating that the efficiency of numerical damping increases as the artificial oscillations become narrower, was shown in section 3.2.1 and will be also shown in section 3.2.5.

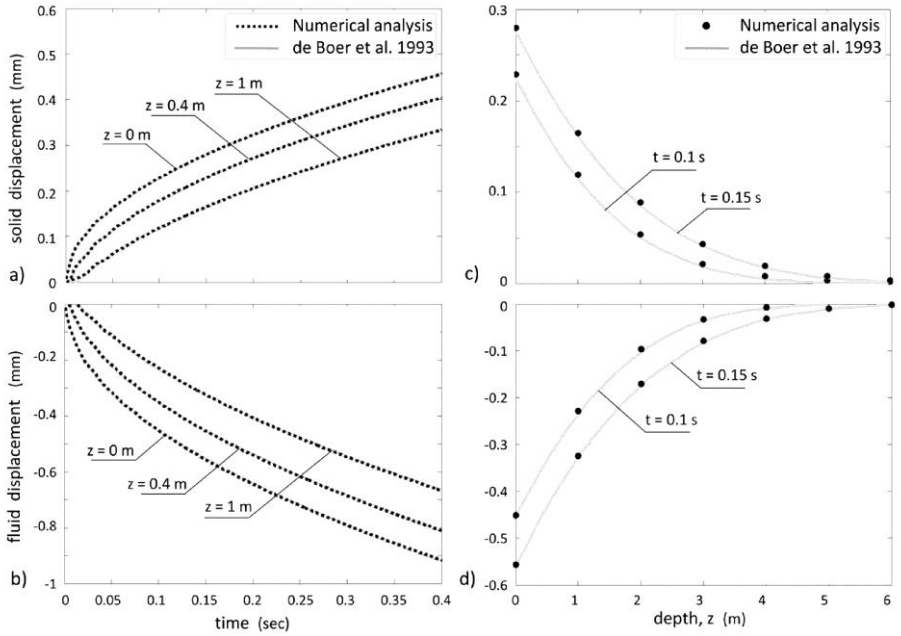

Fig. 12 Comparison between numerical analysis and analytical solution by de Boer *et al*. (1993) in terms of (a) solid displacements versus time at different depths, (b) fluid displacements versus time at different depths, (c) solid displacements versus depth at different times, and (d) fluid displacements versus depth at different times

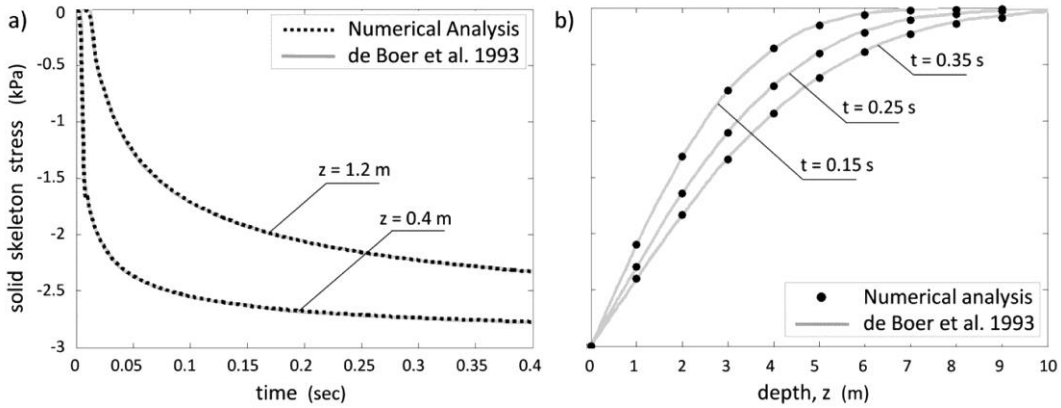

Fig. 13 Comparison between numerical analysis and analytical solution by de Boer *et al*. (1993) in terms of (a) solid–skeleton stress versus time at different depths, and (b) solid–skeleton stress versus depth at different times

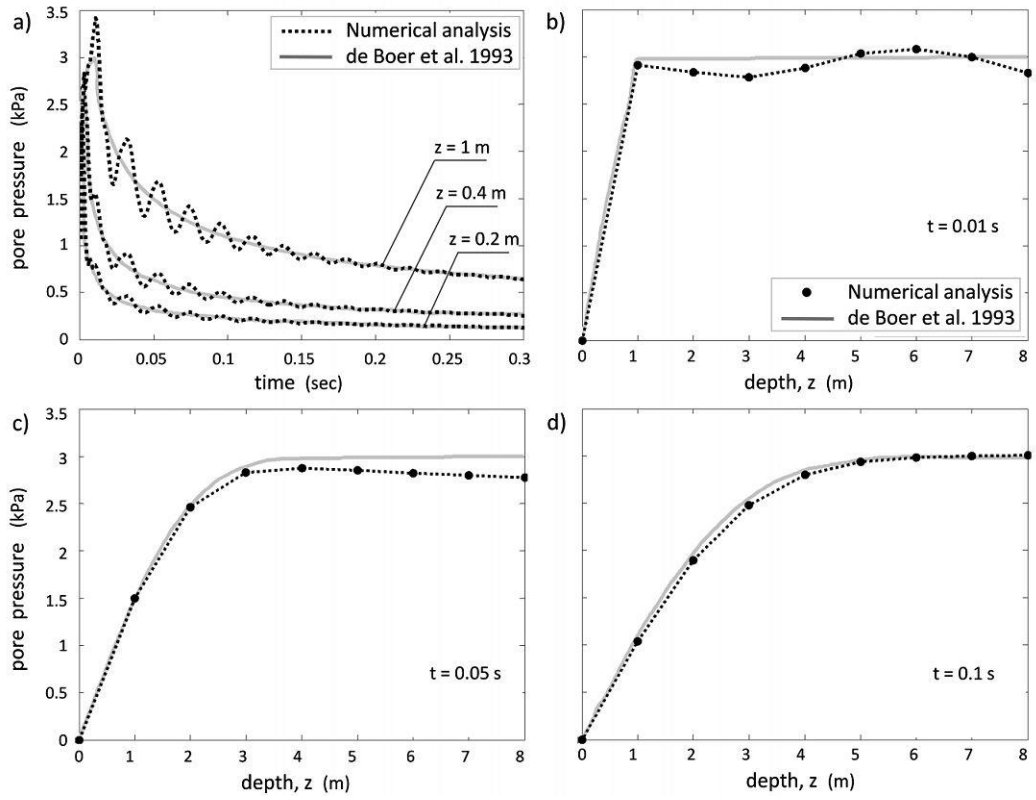

Fig. 14 Comparison between numerical analysis and analytical solution by de Boer *et al.* (1993): (a) pore fluid pressure versus time at different depths, (b) pore fluid pressure stress versus depth at time t = 0.01 sec, (c) pore fluid pressure stress versus depth at time t = 0.05 sec, and (d) pore fluid pressure stress versus depth at time t = 0.1 sec

3.2.4 Sinusoidal loading

Numerical example for the sinusoidal loading case was also used to verify implementation of u–p–U formulation. The frequency of the excitation is equal to 75 rad/s and the load is given by the function $3\left(1-\cos\left(75t\right)\right)$ 3 × (1 − cos(75 × t)). Table 2 shows the soil properties of the numerical model, which are the same as in the previous section. The value of Darcy permeability assigned to the soil skeleton is again equal to 0.01 m/s.

The minimum wave velocity that can be present in the model can be approximately estimated by equation

$$V_{min} = \sqrt{\frac{M}{\left(1-n\right)\rho_s}} = 128?m/s \tag{34}$$

corresponding to a dry solid skeleton. Thus, the minimum wavelength can be estimated by Eq. (30) as 10.7 m leading to a maximum element size of 1.07 m. The numerical grid used for the simulation

of the 1– D shock wave propagation consists of 100 u–p–U brick finite elements of dimensions 10 cm×10 cm×10 cm creating a soil column 10 m high. The maximum time-step required is estimated by Eq. (31) equal to 4×10^{-6} sec approximately for the selected element size. The Newmark parameters were selected to be: $\gamma = 0.6$ and $\beta = 0.3025$, in order to introduce numerical damping. At the top surface of the soil column, the sinusoidal loading is applied to the solid part through four nodal loads at the top.

Fig. 15 depicts the time-histories of solid and fluid displacements, as well as pore pressure and ef- fective stress as obtained by both numerical analysis and analytical solution. Numerical analysis captures the response of fully saturated soil under sinusoidal loading in a satisfactory manner. In particularly, the solid displacement gradually accumulates downwards while the fluid is squeezed out of the skeleton. However, there are moments of partial recovery, when the load on the surface decreases, which renders the pore pressure values negative close to surface, as the fluid is absorbed inwards (suction). The effective stress seems to be more sensitive to loading close to the surface following the shape of the excitation, whereas the effect tends to diminish for greater depths due to solid-fluid interaction.

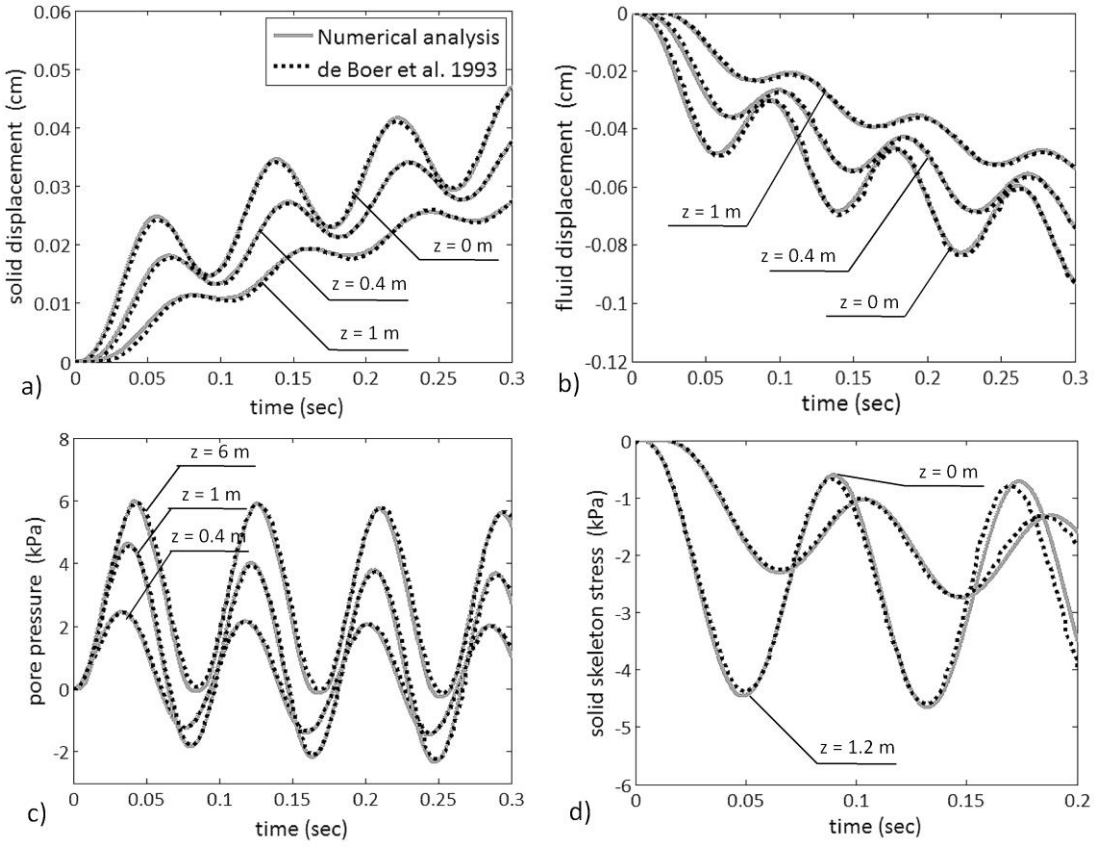

Fig. 15 Comparison between numerical analysis and analytical solution by de Boer *et al*. (1993) in terms of (a) solid displacements, (b) fluid displacements, (c) pore pressure and (d) solid skeleton stress versus time for different depths

3.2.5 Step velocity excitation

Semi–Analytical Solution by Hiremath *et al*. (1988) – Hiremath *et al*. (1988) present a semi–analytical solution of Biot's equations of motion for one-dimensional wave propagation in a fluid-saturated linear elastic isotropic medium (soil) using Laplace transformation followed by numerical inversion. This study is considered to be an extension of the exact transient solution presented by Garg *et al*. (1974) for two limiting cases of infinitely small and infinitely large viscous coupling. In both cases, a soil column offinite dimension (50 cm) subjected to velocity boundary conditions at the surface was analyzed, allowing for reflection of waves at the boundaries.

One of the most important observations, made by both Garg *et al*. (1974) and Hiremath *et al*. (1988), is that in case of strong viscous coupling (high drag), the material behaves as a single continuum with internal dissipation and the two wave fronts tend to become a single one.

In particular, Hiremath *et al*. (1988) examined two cases allowing for small and large viscous coupling. Moreover, two different types of excitations were applied at the boundary surface in terms of solid and fluid velocity. In the first case, a unit step boundary condition was applied at the top surface for both solid and fluid phases (to be studied below). In the second case, the fluid velocity applied at the boundary is slightly different from the applied solid velocity, and it is increasing gradually to unity over a short time scale. The results obtained from the numerical inversion allowed for six reflections of the fast compressional wave of first kind and two reflections of the secondary slow longitudinal wave.

Numerical Analysis – Models for two extreme values of viscous coupling: a) large ($k = 0.148 \times 10^{-8}$ cm^{3}s/g) and b) low ($k = 0.148 \times 10^{-2}$ cm^{3}s/g) are developed and simulated. At the top surface of the soil column, a step velocity of 1.0 × 10−2 m/s is applied both to the solid and the fluid phase. Only the vertical translational degrees of freedom are free so that no lateral flow or displacement is allowed. The base of the model is rigid and impervious. A step excitation introduces all frequencies in the model, requiring a very small element size (theoretically, based on Eq. (30), the element size should really be infinitely small, in order to accommodate all introduced frequencies). The selected finite element mesh consists of 100 u–p–U brick finite elements of dimensions 0.005 m × 0.005 m × 0.005 m creating a soil column 50 cm high, as suggested by Hiremath *et al*. (1988). Table 2 shows the soil properties used for this model. The solid skeleton is so rigid that the wave of the first kind propagates with a velocity close to 3500 m/s according to equation Eq. (33). The required time step is estimated by Eq. (31) and is equal to $\Delta t = 1.4 \times 10^{-6}$ sec. The selected temporal integration involves 1972 steps of $\Delta t = 5.0 \times 10^{-7}$ sec. The Newmark set of parameters was selected as $\gamma = 0.6$ and $\beta = 0.3025$, introducing numerical damping in the model.

Figs. 16 and 17 show the comparison between numerical and analytical results for both extreme cases of viscous coupling. Overall, the finite element solution reproduces correctly the trends of wave propagation in both limiting cases of viscous coupling. In particular, numerical analysis demonstrates well that for the case of strong viscous coupling, solid and fluid velocities are in phase with each other.

In order to improve the accuracy of the numerical solution, a finer spatial and temporal discretization was used, with $\Delta h = 0.001$ m and $\Delta t = 2 \times 10^{-7}$ sec, while Newmark parameters remained the same. Fig. 18 depicts the analytical solution versus the numerical results obtained from both meshes. Evidently, the finer mesh achieves a greater accuracy, suppresses oscillations, and gives a more similar response to the analytical solution, as expected. It is interesting to notice that when numerical damping is used, all artificial oscillations are suppressed in case of finer mesh, while they persist in case of coarser mesh, as illustrated in Fig. 19.

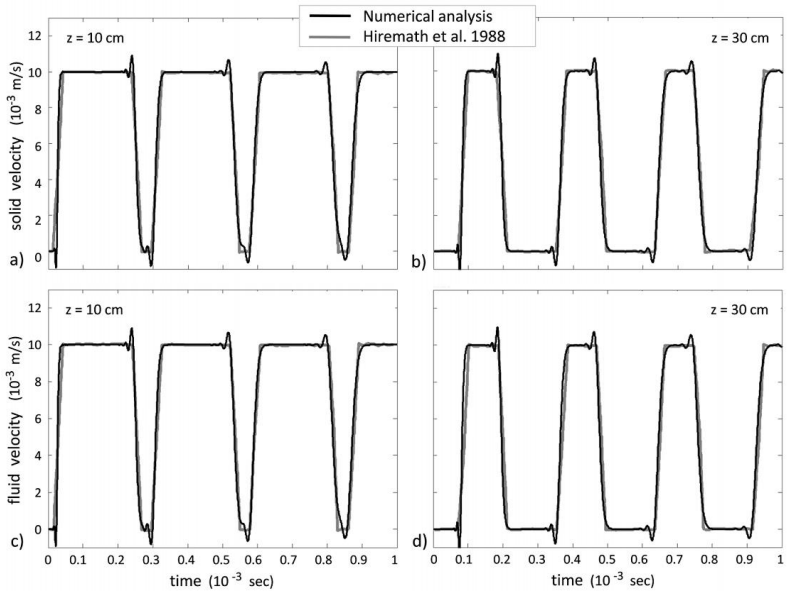

Fig. 16 Comparison between numerical analysis and analytical solution Hiremath *et al.* (1988) for the case of strong viscous coupling ($k = 0.148 \times 10^{-8}$ cm^{3}s/g) in terms of time histories of: (a) solid velocity at 10 cm below the surface, (b) solid velocity at 30 cm below the surface, (c) fluid velocity at 10 cm below the surface and and (d) fluid velocity at 30 cm below the surface

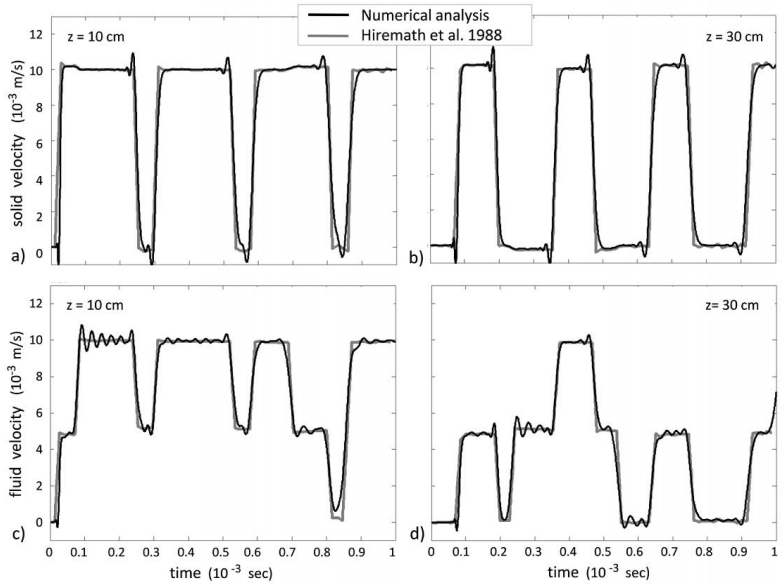

Fig. 17 Comparison between numerical analysis and analytical solution Hiremath *et al*. (1988) for the case of strong viscous coupling ($k = 0.148 \times 10^{-2}$ cm^{3}s/g) in terms of time histories of: (a) solid velocity at 10 cm below the surface, (b) solid velocity at 30 cm below the surface, (c) fluid velocity at 10 cm below the surface and and (d) fluid velocity at 30 cm below the surface

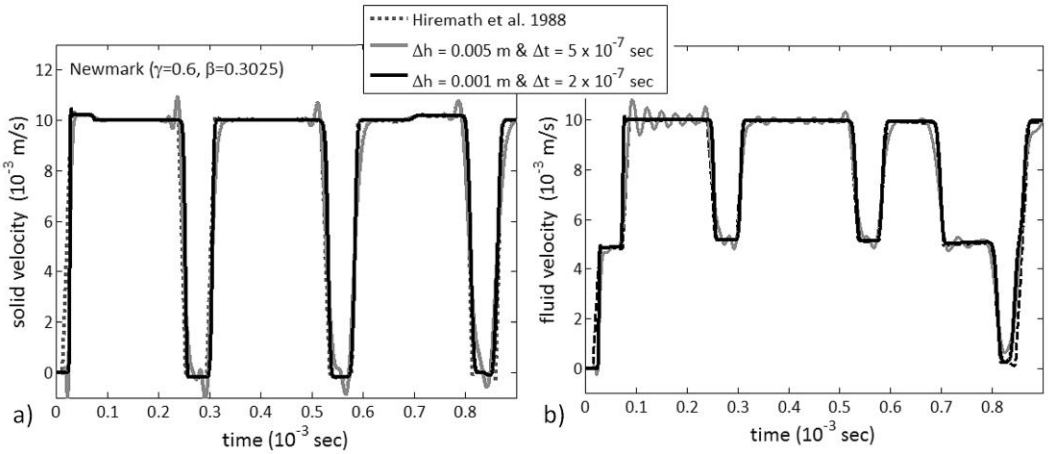

Fig. 18 Analytical solution by Hiremath *et al*. (1988) versus numerical analysis, for two different combinations of spatial/temporal discretization, in case of weak viscous coupling ($k = 0.148 \times 10^{-2}$ cm^{3}s/g): (a) solid velocity at 10 cm below the surface and (b) fluid velocity at 10 cm below the surface, with time. Numerical damping was introduced in the analysis ($\gamma = 0.6$ and $\beta = 0.3025$)

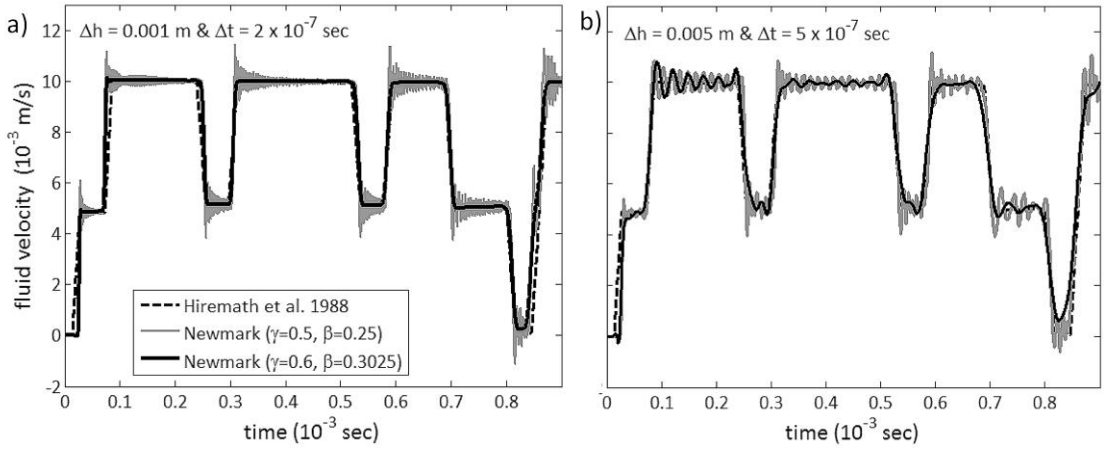

Fig. 19 Analytical solution by Hiremath *et al*. (1988) versus numerical analysis, for two different combinations of spatial/temporal discretization and numerical damping, in case of weak viscous coupling ($k = 0.148 \times 10^{-2}$ cm^{3}s/g) and in terms of fluid velocity time histories at 10 cm below the surface

4. Conclusions

A solution verification suite for modeling and simulation of fully coupled behavior of saturated porous media, using *u-p-U* formulation, has been presented in this paper. Analytical solutions for both static and dynamic examples have been included in this suite. Detailed comparison between numerical and analytical solutions shows close matching, while common numerical discretization effects are captured and controlled. In particular, artificially–introduced (by discretization)

higher-frequency effects have been observed, as in most numerical simulations. These numerical dispersion effects have been investigated focusing on the influence of numerical features such as spatial and temporal refinement, as well as numerical damping on the obtained response. It is illustrated that the finer meshes better approach the analytical solutions, as expected; however, such finer meshes produce even higher frequency (artificial) oscillations. It is also shown that such oscillations produced by finer meshes c can be more efficiently damped out numerically than those produced by coarser discretization.

Presented solution verification suite can be used by any modeling and simulation effort that deals with the response of fully saturated porous media. In this particular case, presented solution verification results provide evidence that the fully coupled models for saturated porous media, from the UCD Computational Geomechanics Group numerical libraries, are solved correctly for both static and dynamic cases.

It is important to observe that any numerical method develop to model and simulation behavior of solids/structures and fluids needs to be verified (and validated if quality experimental data is available). Only after such verification (and validation) process has been successfully completed, a method can be claimed to be complete. The main aim of this paper, with presented verification of the u-p-U formulation, is to contribute to such approach to numerical modeling and simulations.

References

Argyris, J. and Mlejnek, H.P. (1991), *Dynamics of Structures*. North Holland in USA Elsevier.

Biot, M. (1941), "General theory of three-dimensional consolidation", *J. Appl. Phys.*, **12**(2), 155-164.

Biot, M. (1955), "Theory of elasticity and consolidation for a porous anisotropic solid", *J. Appl. Phys.*, **26**(2), 182-185.

Biot, M. (1956a), "Theory of deformation of a porous viscoelastic anisotropic solid", *J. Appl. Phys.*, **27**(5), 459-467.

Biot, M. (1956b), "Theory of propagation of elastic waves in a fluid-saturated porous solid. i. low-frequency range", *J. Acoust. Soc. Am.*, **28**(2), 168-178.

Biot, M. (15956c), "Theory of propagation of elastic waves in a fluid-saturated porous solid. ii. higher frequency range", *J. Acoust. Soc. Am.*, **28**(2), 179-191.

Bowen. R. (1980), "Incompressible porous media models by use of the theory of mixtures", *Int. J. Eng. Sci.*, **18**, 1129-1148.

Bowen, R. (1982), "Compressible porous media models by use of the theory of mixtures", *Int. J. Eng. Sci.*, **20**(6), 697-735.

Coussy, O. (1995), *Mechanics of Porous Continua*, John Wiley and Sons.

Coussy, O. (2004), *Poromechanics*. John Wiley and Sons, Chichester.

de Boer, R., Ehlers, W. and Liu, Z. (1993), "One-dimensional transient wave propagation in fluid-saturated incompressible porous media", *Arch. Appl. Mech.*, **63**(1), 59-72.

Deraemaeker, P.B.A. and Babuska, I. (1999), "Dispersion and pollution of the FEM solution for the Helmholtz equation in one, two and three dimensions", *Int. J. Numer. Meth. Eng.*, **46**(4), 471-499.

Ehlers, W. (1993), "Compressible, incompressible and hybrid two-phase models in porous media theories", *ASME: AMD*, **158**, 25-38.

Gajo, A. (1995), "Influence of viscous coupling in propagation of elastic waves in saturated soil", *J. Geotech. Eng.- ASCE* , **121**(9), 636-644.

Gajo, A. and Mongiovi, L. (1995), "An analytical solution for the transient response of saturated linear elastic porous media", *Int. J. Numer. Anal. Meth. Geomech.*, 19(6), 399-413.

Gajo, A., Saetta, A. and Vitaliani, R. (1994), "Evaluation of three– and two–field finite element methods

for the dynamic response of saturated soil", *Int. J. Numer. Meth. Eng.*, **37**, 1231-1247.
Garg, S. K., Nayfeh, H. and Good, A.J. (1947), "Compressional waves in fluid-saturated elastic porous media", *J. Appl. Phys.*, **45**(5), 1968-1974.
Hiremath, M.S., Sandhu, R.S., Morland, L.W. and Wolfe, W.E. (1988), "Analysis of one-dimensional wave propagation in a fluid-saturated finite soil column", *Int. J. Numer. Anal. Meth. Geomech.*, **12**, 121-139.
Hughes, T. (1987), *The Finite Element Method ; Linear Static and Dynamic Finite Element Analysis*. Prentice Hall Inc.
Ihlenburg, F. and Babuška, I. (1955), "Dispersion analysis and error estimation of Galerkin finite element methods for the Helmholtz equation", *Int. J. Numer. Meth. Eng.*, **38**, 3745-3774.
Jeremić, B., Cheng, Z., Taiebat, M. and Dafalias, Y.F. (2008), "Numerical simulation of fully saturated porous materials", *Int. J. Numer. Anal. Meth. Geomech.*, **32**(13), 1635-1660.
Newmark, N.M. (1959), "A method of computation for structural dynamics", *J. Eng. Mech. Div.- ASCE*, **85**, 67-94.
Oberkampf, W.L., Trucano, T.G. and Hirsch, C. (2002), "Verification, validation and predictive capability in computational engineering and physics", *Proceedings of the Foundations for Verification and Validation on the 21st Century Workshop*, pages 1-74, Laurel, Maryland, October 22-23 2002. Johns Hopkins University / Applied Physics Laboratory.
Oden, T., Moser, R. and Ghattas, O. (2010a), "Computer predictions with quantified uncertainty, part I", *SIAM News*, **43**(9).
Oden, T., Moser, R. and Ghattas, O. (2010b), "Computer predictions with quantified uncertainty, part II", *SIAM News*, **43**(10).
Roy, C.J. and Oberkampf. W.L. (2011), "A comprehensive framework for verification, validation, and uncertainty quantification in scientific computing", *Comput. Method. Appl. M.*, **200**(25-28), 2131-2144, doi: 10.1016/j.cma.2011.03.016.
Schanz, M. (2009), "Poroelastodynamics: Linear models, analytical solutions, and numerical methods", *Appl. Mech. Rev. - ASME*, **62**, 030803–1 – 030803–15.
Semblat, J.F. and Brioist, J.J. (2000), "Efficiency of higher order finite elements for the analysis of seismic wave propagation", *J. Sound Vib.*, **231**(2), 460-467.
Simon, B.R., Wu, J.S., Zienkiewicz, O.C. and Paul, D.K. (1984), "Evaluation of $u - w$ and $u - \pi$ finite element methods for the dynamic response of saturated porous media using one–dimensional models", *Int. J. Numer. Anal. Meth. Geomech.*, **10**, 461-482.
Tasiopoulou, P., Taiebat, M., Tafazzoli, N. and Jeremić, B. (2014), "On validation of fully coupled behavior of porous media using centrifuge test results", *Coupled Syst. Mech.*, In Review.
Terzaghi, K. (1923), "Die berechnung der durchlassigkeitsziffer des tones aus dem verlauf der hydrodynamischen spannungserscheinungen", *Sitz. Akad. Wissen., Wien Math. Naturwiss. Kl., Abt.IIa*, **132**, 105-124.
Terzaghi, K. (1943), *Theoretical Soil Mechanics*, Wiley, New York.
Zienkiewicz, O.C. and Shiomi, T. (1984), "Dynamic behaviour of saturated porous media; the generalized Biot formulation and its numerical solution", *Int. J. Numer. Anal. Meth. Geomech.*, **8**, 71-96.
Zienkiewicz, O.C. and Taylor, R.L. (1991a), *The Finite Element Method*, volume 1, McGraw - Hill Book Company, fourth edition.
Zienkiewicz, O.C. and Taylor, R.L. (1991b), *The Finite Element Method*, volume 2, McGraw - Hill Book Company, Fourth edition.

Appendix A. Finite Element Formulation

Standard finite element discretization (Zienkiewicz and Taylor 1991a,b), using shape functions, is used to describe each of the unknown fields (u–p–U) in terms of nodal values (solid displacements, $\bar{u}_{Ki}$, pore fluid pressures, $\bar{p}_K$ and pore fluid displacements, $\bar{U}_{Ki}$)

$$u_i N_K^u \bar{u}_{Ki}, \quad p = N_K^p \bar{P}_K \, U_i = N_K^U \bar{U}_{Ki} \tag{35}$$

where N_K^u, N_K^p and N_K^U are (in this case same) shape functions for solid displacement, pore pressure and fluid displacement, respectively. Each node of the (u–p–U) element thus features seven degrees of freedoms in three dimensions (three for solid displacements, one for pore fluid pressures, and three or pore fluid displacements). It should be noted that it is possible to use same shape functions for both displacement and pore pressure unknown field as the u–p–U formulation with compressible fluid allows that without volumetric locking.

By using finite element discretization and after some tensor algebra and manipulations, the weak form of governing equations can be obtained from the strong form described by Eqs. (4)-(6)

$$\begin{aligned}
&\begin{bmatrix} (M_s)_{KijL} & 0 & 0 \\ 0 & 0 & 0 \\ 0 & 0 & (M_f)_{KijL} \end{bmatrix} \begin{bmatrix} \ddot{\bar{u}}_{Lj} \\ \ddot{\bar{p}}_N \\ \ddot{\bar{U}}_{Lj} \end{bmatrix} + \begin{bmatrix} (C_1)_{KijL} & 0 & -(C_2)_{KijL} \\ 0 & 0 & 0 \\ -(C_2)_{Ljik} & 0 & (C_3)_{KijL} \end{bmatrix} \begin{bmatrix} \dot{\bar{u}}_{Lj} \\ \dot{\bar{p}}_N \\ \dot{\bar{U}}_{Lj} \end{bmatrix} \\
&+ \begin{bmatrix} 0 & -(G_1)_{KiM} & 0 \\ -(G_1)_{LjM} & -P_{MN} & -(G_2)_{LjM} \\ 0 & -(G_2)_{KiL} & 0 \end{bmatrix} \begin{bmatrix} \bar{u}_{Lj} \\ \bar{p}_M \\ \bar{U}_{Lj} \end{bmatrix} \\
&+ \begin{bmatrix} \int_\Omega N_{K,j}^u \sigma'_{ij} \, dV \\ 0 \\ 0 \end{bmatrix} - \begin{bmatrix} \bar{f}_{Ki}^u \\ 0 \\ \bar{f}_{Ki}^U \end{bmatrix} = 0
\end{aligned} \tag{36}$$

where the left hand side components are

$$\begin{aligned}
(M_s)_{KijL} &= \int_V N_K^u (1-n) \rho_s \delta_{ij} N_L^u dV \quad ; \quad (M_f)_{KijL} = \int_V N_K^U n \rho_f \delta_{ij} N_L^u dV \\
(C_1)_{KijL} &= \int_V N_K^u n^2 k_{ij}^{-1} N_L^u d\nu \quad ; \quad (C_2)_{KijL} = \int_V N_K^u n^2 k_{ij}^{-1} N_L^U dV \\
(C_3)_{KijL} &= \int_V N_K^U n^2 k_{ij}^{-1} N_L^U dV \quad ; \quad (G_1)_{KiM} = \int_V N_{K,i}^u (\alpha - n) N_M^p dV \\
(G_2)_{KiM} &= \int_V n N_{K,i}^U N_M^p dV \quad ; \quad P_{NM} = \int_V N_N^p \frac{1}{Q} N_M^p dV
\end{aligned} \tag{37}$$

while the right hand side are

$$
\begin{aligned}
(\bar{f}_s)_{Ki} &= \int_{A_t} N_K^u \sigma'_{ij} n_j \mathrm{d}A - \int_{A_p} N_K^u (\alpha - n) p n_i \mathrm{d}A + \int_V N_K^u (1-n)\rho_s b_i \mathrm{d}V \\
(\bar{f}_f)_{Ki} &= -\int_{A_p} N_K^U n p n_i \mathrm{d}A + \int_V N_K^U n \rho_f b_i \mathrm{d}V
\end{aligned}
\tag{38}
$$

where V is the volume, and A_t and A_p are the domain boundaries with traction and the pore fluid pressure defined, respectively.

It is very important to note that the velocity proportional viscous damping was introduced directly through the damping tensor with components $(C_1)_{KijL}$, $(C_2)_{KijL}$ and $(C_3)_{KijL}$, which are functions of porosity and permeability of the skeleton. This damping provides for physically based, velocity proportional energy dissipation due to interaction of pore fluid and the solid (soil) skeleton. It is also emphasized that presented formulation and implementation do not (need to) use Rayleigh damping.

Appendix B. Time Integration

In order to develop integration of dynamic finite element equation in the time domain, Eq. (36) is rewritten in a residual matrix form (Argyris and Mlejnek 1991)

$$
\boldsymbol{R} = \boldsymbol{M}\,\ddot{\boldsymbol{x}} + \boldsymbol{C}\dot{\boldsymbol{x}} + \boldsymbol{K}'\boldsymbol{x} + \boldsymbol{F}(\boldsymbol{x}) - \boldsymbol{f} = 0 \tag{39}
$$

where $x = \{\bar{u}, \bar{p}, \bar{U}\}^T$ represent a vector od generalized unknown variables. Eq. (39) represents the general non-linear form for which the usual tangent stiffness **K** is obtained from

$$
\mathbf{K} = \frac{\partial \mathbf{R}}{\partial \mathbf{x}} = \mathbf{K}' + \frac{\partial \mathbf{F(x)}}{\partial \mathbf{x}} \tag{40}
$$

In the specific case of u–p–U formulation of interest here one can write matrix form

$$
\mathrm{M} = \begin{bmatrix} \mathrm{M_s} & 0 & 0 \\ 0 & 0 & 0 \\ 0 & 0 & \mathrm{M_f} \end{bmatrix}, \quad \mathrm{C} = \begin{bmatrix} \mathrm{C_1} & 0 & -\mathrm{C_2} \\ 0 & 0 & 0 \\ -\mathrm{C_2^T} & 0 & \mathrm{C_3} \end{bmatrix} \tag{41}
$$

$$
\mathrm{K}' = \begin{bmatrix} 0 & -\mathrm{G_1} & 0 \\ -\mathrm{G_1^T} & -\mathrm{P} & -\mathrm{G_2^T} \\ 0 & -\mathrm{G_2} & 0 \end{bmatrix}, \quad \mathrm{K} = \begin{bmatrix} \mathrm{K^{ep}} & -\mathrm{G_1} & 0 \\ -\mathrm{G_1^T} & -\mathrm{P} & -\mathrm{G_2^T} \\ 0 & -\mathrm{G_2} & 0 \end{bmatrix} \tag{42}
$$

where

$$
\boldsymbol{K}^{ep} = \left(K^{ep}\right)_{KijL} = \int_V N^u_{K,m} E^{ep}_{imjn} N^u_{L,n} dV \tag{43}
$$

The above set of residual (nonlinear) dynamic equations is solved using the Newmark procedure (Newmark 1959). This time integration method has two parameters, β and γ, and is described by the

following two equations

$$^{n+1}x = {}^{n}x + \Delta t\,{}^{n}x + \Delta^2 t\left[\left(\frac{1}{2}-\beta\right){}^{n}\ddot{x} + \beta\,{}^{n+1}\ddot{x}\right] \tag{44}$$

$$^{n+1}\dot{x} = {}^{n}\dot{x} + \Delta t\left[\left(1-\gamma\right){}^{n}\ddot{x} + \gamma\,{}^{n+1}\ddot{x}\right] \tag{45}$$

which give the relations between the current time step n to the next time step $n + 1$. The method is generally an implicit method, except when both β and γ are zero. If the parameters β and γ satisfy the following conditions:

$$\gamma \geq \frac{1}{2},\ \ \beta = \frac{1}{4}(\gamma + \frac{1}{2})^2 \tag{46}$$

the time integration method is unconditionally stable. Any γ value greater than 0.5 will introduce numerical damping. Well-known members of the Newmark time integration method family include: trapezoidal rule or average acceleration method for $\beta = 1/4$ and $\gamma = 1/2$, linear acceleration method for $\beta = 1/6$ and $\gamma = 1/2$, and (explicit) central difference method for $\beta = 0$ and $\gamma = 1/2$. If and only if $\gamma = 1/2$, it is second order accurate (Hughes 1987).